

Testing the role of AGN on the star formation and metal enrichment of “twin galaxies”

J. Angthopo^{1*}, I. del Moral-Castro^{2,3}, I. Ferreras^{2,3,4}, B. García-Lorenzo^{2,3}
and C. Ramos Almeida^{2,3}

¹ Mullard Space Science Laboratory, University College London, Holmbury St Mary, Dorking, Surrey RH5 6NT, UK

² Instituto de Astrofísica de Canarias, Calle Vía Láctea s/n, E38205, La Laguna, Tenerife, Spain

³ Departamento de Astrofísica, Universidad de La Laguna (ULL), E-38206 La Laguna, Tenerife, Spain

⁴ Department of Physics and Astronomy, University College London, Gower Street, London WC1E 6BT, UK

ABSTRACT

We explore the effect of AGN activity on the star formation history of galaxies by analysing the stellar population properties of ten pairs of nearby twin galaxies – selected as being visually similar except for the presence of an AGN. The selection of such twin samples represents a method to study AGN feedback, as recently proposed by del Moral Castro et al. We use integral field unit (IFU) data from CALIFA, stacked within three fixed apertures. AGN galaxies in a twin pair suggest more evolved stellar populations than their non-AGN counterpart 90% of the time, regardless of aperture size. A comparison with a large sample from SDSS confirms that most twins are representative of the general population, but in each twin the differences between twin members is significant. A set of targeted line strengths reveal the AGN member of a twin pair is older and more metal rich than the non-AGN galaxy, suggesting AGN galaxies in our sample may either have an earlier formation time or follow a different star formation and chemical enrichment history. These results are discussed within two simple, contrasting hypotheses for the role played by AGN in galaxy evolution, which can be tested in the future at a greater detail with the use of larger data sets.

Key words: galaxies: evolution – galaxies: formation – galaxies: interactions – galaxies: stellar content.

1 INTRODUCTION

While substantial progress has been made over the past decades in the subject of galaxy formation and evolution, many questions remain unanswered, due to the complexity of the underlying physics, and the limitations of both observations and simulations. The advance in our understanding of this field has been facilitated through the use of high quality surveys, from the classic imaging and spectroscopic data of SDSS (York et al. 2000) to the full 3D capability of IFU-based surveys, such as, e.g., ATLAS^{3D} (Cappellari et al. 2011), CALIFA (Sánchez et al. 2012), MaNGA (Bundy et al. 2015), or SAMI (Croom et al. 2021), as well as through cosmological hydrodynamical simulations, such as EAGLE (Schaye et al. 2015) or IllustrisTNG (Marinacci et al. 2018; Nelson et al. 2018; Springel et al. 2018; Pillepich et al. 2018). High quality survey data help us discern the various trends found in galaxy properties, while the simulations, constrained by the observations, enable us to gain a

physical interpretation of the key mechanisms driving galaxy formation and evolution.

There have been a number of prominent discoveries in the past few decades, one of the key results being the presence of a bimodal distribution in galaxies (e.g. Strateva et al. 2001). This bimodality is the result of a distinct presence of two main types of galaxies: star-forming (SF) and quiescent (Q) galaxies. SF galaxies are in the process of formation, and at lower redshift they have preferentially lower stellar mass, appear blue in optical bands, have high star formation rates (SFR) and have significant amounts of cool gas and dust. In contrast, Q galaxies represent an evolved version of SF galaxies (Faber et al. 2007), as they are older, appear red in the visible spectrum, have little to no ongoing star formation and have very little cool gas and dust. Morphologically, SF galaxies are mainly disc/spiral and Q galaxies are mostly classified as early-types. Bimodality has been observed in various planes, such as the colour-magnitude (Graves et al. 2007), SFR-mass (Schiminovich et al. 2007), UVJ bicolour (Williams et al. 2009), colour-mass (Schawinski et al. 2014) and 4000Å break-velocity dispersion (Angthopo et al. 2019, hereafter A19) diagrams.

* E-mail: james.angthopo.16@ucl.ac.uk

The bimodal distribution can be split into three key distinct regions in a colour-mass plane. The two main areas are the Blue Cloud (BC), mostly occupied by SF galaxies, and the Red Sequence (RS), where most of the Q galaxies lie (Strateva et al. 2001; Baldry et al. 2004; Wyder et al. 2007). Between these two exists a sparse region known as the Green Valley (GV). The GV represents an essential stage of galaxy evolution, as this is where transitioning galaxies are thought to reside (e.g. Salim 2014). Galaxies on the GV are affected by key physical mechanisms associated with halting star formation, and their spectra encode information about the timescales related to these processes. It is generally assumed that galaxies evolve from the BC to the RS through the GV, and the sparsity of the latter suggests a fast transition (Bremer et al. 2018; Nelson et al. 2018; Díaz-García et al. 2019; Phillipps et al. 2019; Anghopo et al. 2020, hereafter A20). However, this image is complicated as quiescent galaxies can go through various episodic phases of star formation, moving them from RS to GV or even BC, if a fresh supply of gas drives additional stages of recent star formation (Kaviraj et al. 2007; Thomas et al. 2010). Galaxy evolution is further complicated as the dominant quenching mechanism varies depending on the stellar mass of galaxies. At low stellar mass, $\lesssim 10^{10.3} M_{\odot}$, stellar feedback is thought to quench star formation in a short period of time (Mathews & Baker 1971; White & Frenk 1991; Hayward & Hopkins 2017). In contrast, at high stellar mass, $\gtrsim 10^{10.3} M_{\odot}$, AGN and major mergers are thought to play an important role in quenching of star formation (Wright et al. 2019; Barišić et al. 2019; Correa et al. 2019; Dashyan et al. 2019; Terrazas et al. 2020; Anghopo et al. 2021).

Even though it has become apparent that AGN are necessary to quench star formation in massive galaxies (Croton et al. 2006; Schaye et al. 2015; Springel et al. 2017), a detailed understanding of how AGN operate and the exact impact they have on the host galaxies has yet to be achieved. On the one hand, the triggering of strong nuclear activity is thought to occur through galaxy-galaxy interactions or mergers, where the supermassive black hole (SMBH) is supplied with fresh gas (Barnes & Hernquist 1991; Heckman & Best 2014). On the other hand, more recent observational results have shown that such processes can occur through secular evolution, where there is no strong evidence of past mergers (Cisternas et al. 2011; Kocevski et al. 2012; Simmons et al. 2013). Due to either of these processes, it is strongly thought that SMBH co-evolve with its host galaxy (Ho 2008; Kormendy & Ho 2013). This co-evolution occurs, as SMBHs grow by accretion of the surrounding gas (Soltan 1982), which in turn feeds an energetic process. This will regulate the growth of the galaxy, as the surrounding gas will be heated or removed to such extent that the star formation is halted (Silk & Rees 1998). There have been many results strengthening this hypothesis. One such key result has been the high fraction of AGN found in the GV, as defined by the colour-magnitude (Martin et al. 2007), colour-mass (Lacerda et al. 2020) and 4000\AA break-velocity dispersion diagram (A19). Note that the general high fraction of AGN in the GV, shows that not only are AGN the cause of star formation quenching, following the so called 'quasar mode', but they also inhibit further onset of star formation by preventing the cooling of gas, through 'maintenance mode' feedback (Ho 2008).

Other than finding out how AGN operate, one of the key questions pertains to their universality. The prominent hypothesis dictates that all galaxies will experience a phase where they undergo on-off cycles of AGN activity (Schawinski et al. 2015). An alternative hypothesis proposes, that not all galaxies will undergo an AGN phase, making AGN galaxies somewhat unique. The different models should result in very different properties of galaxies. Therefore in this paper, we make use of a sample of twin galaxies that are expected to differ only by the presence/absence of an AGN (del Moral-Castro et al. 2020) to test these scenarios. In Sec. 2, we present the data and discuss the methodology. Sec. 3 contrasts the properties of AGN and non-AGN galaxies in the twin samples. Sec. 4 presents a physical interpretation of our results in the framework of two simple and alternative scenarios, and also discusses the potential caveats in the interpretation of the results. Finally Sec. 5 summarizes the main results of this paper and its implication for future studies. To avoid confusion, all apertures defined in the paper are quoted by *radius*, unless specifically stated.

2 METHODOLOGY

2.1 CALIFA data and twin galaxy selection

For the selection of twins, which refers to two galaxies that are almost identical in overall appearance and are similar in general properties, such as mass, luminosity, ellipticity and morphology, we make use of the 3D optical data (third Data release) of the Calar Alto Legacy Integral Field Area survey (hereafter CALIFA, Sánchez et al. 2012, 2016). The CALIFA survey observed ~ 667 galaxies within redshift $0.005 \lesssim z \lesssim 0.03$. The parent sample was reduced to 404 galaxies by Méndez-Abreu et al. (2017), who disregarded those that presented signs of interaction, merging activity, or had a high inclination angle ($i > 70^{\circ}$), for a reliable characterisation of morphology. Furthermore, they also check for presence of bright stars that could contaminate the systems. For each target that we choose to study, the survey provides three data cubes: V500, V1200, and COMBO. The V500 data cubes have low spectral resolution, covering a wavelength range of $3745 < \lambda < 7500 \text{\AA}$ with $R \sim 850$ at $\lambda \sim 5000 \text{\AA}$. The V1200 data cubes have higher resolution but cover a narrower spectral window, $3650 < \lambda < 4840 \text{\AA}$ with $R \sim 1650$ at $\lambda \sim 4500 \text{\AA}$. The COMBO data cubes are a combination of the high and low resolution data cubes, where the high resolution spectra, via convolution with a smoothing kernel, are degraded to match the lowest resolution spectra of the sample. The combined data cubes are produced to overcome the vignetting affecting the other sets.

We give below a brief description of the selection process of twin galaxies - differing in nuclear type. More details can be found in the papers presenting the original definition (del Moral-Castro et al. 2019, 2020). We start with the selection of the AGN sample, identified with the ratios of emission line luminosities, applying the standard BPT classification method (Baldwin et al. 1981). The lines are isolated making use of the fitting codes pPXF (Cappellari & Emsellem 2004) and GANDALF (Sarzi et al. 2006; Falcón-Barroso et al. 2006). An AGN is selected if the data meet the required criteria for a Seyfert galaxy in all four different BPT diagrams - three

defined in Kewley et al. (2001) and one defined in Cid Fernandes et al. (2010), that compare the line ratios $[\text{OIII}]/\text{H}\beta$, $[\text{NII}]/\text{H}\alpha$, $[\text{SII}]/\text{H}\alpha$, $[\text{OI}]/\text{H}\alpha$, and $[\text{OIII}]/[\text{OII}]$. The AGN galaxies are included in the sample only if they are considered to be isolated. Following the isolation criteria detailed in Barrera-Ballesteros et al. (2014), from the whole CALIFA sample, galaxies are discarded if they meet all three criteria: (i) they have neighbouring galaxies within 250 kpc (ii) they have neighbours with a systemic velocity difference smaller than 1000 km s^{-1} (iii) their SDSS r -band magnitude difference, with the neighbouring galaxy, is less than 2 mag. The original sample was assembled to study the resolved galactic properties (del Moral-Castro et al. 2019). This original sample was expanded upon, where the differences in angular momentum was explored (del Moral-Castro et al. 2020). In addition, only galaxies with a spiral morphology, and types Sa/SBa to Sbc/SBbc are included, thus enforcing a “simpler” mass assembly history, rejecting the effect of major mergers. This selection criteria yielded 19 AGN galaxies.

To find the corresponding twin galaxies to these AGN (hereafter identified as SF galaxies¹), a control sample of star forming galaxies were selected. For the SF galaxy to be considered a twin, firstly they have to be isolated and have to match the Hubble morphology of the AGN galaxy. In addition, the stellar mass difference between AGN and SF galaxies has to be $\Delta \log(M_*/M_\odot) \lesssim 0.25$ dex, the absolute magnitude difference $\Delta M_r \lesssim 0.70$ mag, the difference in SDSS- r band disc ellipticity $\Delta \epsilon \lesssim 0.2$. The selected candidates are then visually inspected to ensure similarity before they are selected as twins. These criteria were imposed in del Moral-Castro et al. (2020), however we further restrict the stellar mass difference to $\Delta \log(M_*/M_\odot) \lesssim 0.20$ dex and introduce a velocity dispersion constraint, where the difference in velocity dispersion in the central region, within 3 arcsec aperture, $\Delta \sigma \leq 30 \text{ km/s}$. Note the velocity dispersion constraint is less than the typical error of measuring velocity dispersion in CALIFA, however this hard constraint on σ further ensures that these twin pairs, AGN and SF, galaxies are as similar as possible as σ is thought to be one of the fundamental parameters of galaxy evolution (Graves et al. 2010; Ferreras et al. 2019). The final sample comprises 8 AGN galaxies in total and 10 twin pairs – note that sometimes one SF can be associated to more than one AGN galaxy as twin. Tab. 1 shows the twin sample. From left to right each column shows the galaxy name with their morphological classification, their “status” (AGN/SF), the twin pair used in this work, stellar mass and velocity dispersion, star formation rate (SFR) and their spatial scale. Figs. D1 and D2 show the SDSS images of these twins. Finally, the sample is separated into four groups, based on the properties of the evolutionary diagram, discussed below. Note, to treat each group as a unique set, we ensure that each of the SF galaxies only belong to one group.

The imposition of our selection method yields state-of-the-art “twin” samples. Extending this to a larger set to obtain a greater number of “twin” galaxies requires substantially extra work and time. The CALIFA survey observed a

total of ~ 665 galaxies, from which we only find 10 “Twin” pairs. Therefore for a more statistically robust sample, say 100 pairs, we would require a parent sample of ~ 6650 galaxies. While IFU surveys such as MANGA (Bundy et al. 2015) have enough galaxies for this, not all are characterised as homogeneously as in CALIFA.

2.2 Nebular emission correction

Before proceeding with the analysis of the stellar populations, we must ensure we can measure the spectral features accurately. All AGN and SF galaxies mostly have a disc-like morphology, i.e. Sa/SBa to Sbc/SBbc, hence these galaxies have strong emission lines. We correct for nebular emission following the methodology outlined in La Barbera et al. (2013), where we fit each of the observed spectra with linear superpositions of simple stellar populations from the Bruzual & Charlot (2003) population synthesis models, using STARLIGHT (Cid Fernandes et al. 2005). Note the use of different synthesis models, such as eMILES or FSPS (Vazdekis et al. 2016; Conroy & Gunn 2010), produce very similar results. For each spectrum, the best fit is subtracted from the original one. The difference produces the nebular emission component, where the lines are fitted with a Gaussian function. The fitted lines are then removed from the original spectra. However, as all the galaxies in the twin sample have strong emission lines, we opt not to measure the $\text{H}\beta$ index in the analysis of populations, as the subtraction is expected to carry substantial systematic uncertainties.

2.3 SDSS reference sample

This paper studies the properties of the sample of twin galaxies with respect to their evolutionary stage, following A19. We need to define the blue cloud (BC), green valley (GV) and red sequence (RS), with a large sample of galaxy spectra from SDSS (Gunn et al. 2006; Abolfathi et al. 2018). Moreover, the large sample maps the general distribution of galaxies at low redshift, that can be taken as reference to compare the properties of the twin AGN/SF sets. The SDSS data correspond to galaxies with a Petrosian r -band magnitude $14.5 < r_{AB} < 17.7$. The spectral coverage of the SDSS spectrograph spans from 3800-9200Å with resolution $R \equiv \lambda/\Delta\lambda$ of 1500 at 3800Å and 2500 at 9200Å (Smeed et al. 2013). In order to remove a substantial bias from the fixed aperture, we restrict the redshift of the sample within $0.05 \lesssim z \lesssim 0.1$. Furthermore, for our measurements to be robust, we only select galaxies with high signal-to-noise ratio in the r band, $\text{SNr} \gtrsim 10$, leaving us with $\sim 228,000$ spectra. We make use of the GALSPECXTRA catalogue (Brinchmann et al. 2004) to retrieve the stellar mass, BPT classification, and foreground dust. We calculate the $D_n(4000)$ strength using a slight variation of the definition from Balogh et al. (1999):

$$D_n(4000) = \frac{\Phi^R}{\Phi^B}, \text{ where } \Phi^i \equiv \frac{1}{\lambda_2^i - \lambda_1^i} \int_{\lambda_1^i}^{\lambda_2^i} \Phi(\lambda) d\lambda, \quad (1)$$

where $(\lambda_1^B, \lambda_2^B, \lambda_1^R, \lambda_2^R) \equiv (3850, 3950, 4000, 4100) \text{ \AA}$. The spectra are corrected for foreground dust extinction, adopting the standard Milky Way law (Cardelli et al. 1989), tak-

¹ However, note that the AGN galaxies in these systems also feature ongoing star formation. This is just a convention to identify the different twin members.

Table 1. Sample of twin galaxies, produced by identifying similar galaxies, where one of the twin members has an AGN. Cols. 1 and 2 show the galaxy ID and the morphological classification (Walcher et al. 2014). Col. 3 labels them as AGN or star forming (SF) (del Moral-Castro et al. 2020), note that AGN galaxies also show signatures of ongoing star formation. Col. 4 identifies the twin by a number. The total stellar mass (Walcher et al. 2014) and central velocity dispersion (measured within a 3 arcsec aperture) are shown in cols. 5 and 6 (del Moral-Castro et al. 2020), respectively. Finally, cols. 7 and 8 shows the SFR (taken from Catalán-Torrecilla et al. 2015) and scale.

Galaxy (1)	Morph. (2)	Type (3)	Twin (4)	$\log M_*/M_\odot$ (5)	σ (km/s) (6)	SFR ($M_\odot \text{ yr}^{-1}$) (7)	Scale (pc/'') (8)
Group 1							
NGC2253	SBbc	SF	1	10.50	109.1	1.13 ± 0.19	257
NGC1093	SBbc	AGN	1	10.43	107.4	0.89 ± 0.14	349
NGC5947	SBbc	SF	1	10.56	119.3	1.40 ± 0.28	402
NGC6004	SBbc	SF	1	10.63	100.8	1.06 ± 0.18	301
NGC2906	Sbc	AGN	3	10.46	114.0	0.68 ± 0.11	165
NGC0001	Sbc	SF	3,4	10.58	131.9	3.92 ± 1.09	305
NGC2916	Sbc	AGN	4	10.64	149.6	1.90 ± 0.33	276
Group 2							
NGC2639	Sa	AGN	2	11.09	210.8	0.57 ± 0.12	247
NGC0160	Sa	SF	2,6	10.99	216.1	0.43 ± 0.05	349
NGC7311	Sa	AGN	6	10.96	206.9	2.06 ± 0.56	310
Group 3							
NGC7466	Sbc	AGN	7	10.68	128.7	2.85 ± 0.49	509
NGC5980	Sbc	SF	7,8	10.69	121.8	4.31 ± 0.75	320
UGC00005	Sbc	AGN	8	10.74	117.9	4.10 ± 0.71	485
Group 4							
NGC6394	SBbc	AGN	5	10.86	105.8	1.36 ± 0.24	596
UGC12810	SBbc	SF	5	10.81	114.0	3.62 ± 0.93	543

ing the extinction values (A_g) for each galaxy from the SDSS catalogues.

We define the BC, GV and RS, following a data-driven approach, where, for a fixed stellar mass bin, we select only star-forming (SF, BPT = 1) and quiescent (Q, BPT = -1) galaxies. From the distribution of SF and Q galaxies in 4000Å break strength within a bin in stellar mass, we produce a probability distribution function (PDF) for BC (\mathcal{P}_{BC}), and RS (\mathcal{P}_{RS}), respectively – adopting a Gaussian distribution in $D_n(4000)$. Finally, we define the GV in the same manner, where the peak of the GV is assumed to be at the point of intersection between the distribution of BC and RS, such that $\mathcal{P}_{BC} = \mathcal{P}_{RS}$. We define the width of the GV distribution as half of the width of the RS PDF. See A19 and A20 for full details.

2.4 Identifying Type 2 AGN in SDSS spectra

In Section 3.2, we contrast the CALIFA-based sample of twin systems with the general galaxy population from SDSS. For this study, the AGN galaxies in CALIFA have been selected as type 2, whereas the SDSS sample is only classified, regarding AGN activity, through a simpler classification based on the BPT diagram, that does not allow us to distinguish between type 1 and type 2 AGN. We apply an additional selection criterion to those SDSS galaxies classified as having an AGN, to remove all possible type 1 AGN. The motivation for this is derived from recent studies indicating that type 1 and 2 AGN may not be just explained by a difference in orientation (see, e.g., Ramos Almeida et al. 2011; Villarroel & Korn 2014; Spinoglio & Fernández-Ontiveros 2021;

Gkini et al. 2021), in contrast to the unification model (e.g., Antonucci 1993).

Previous studies from the literature typically impose a threshold in the width of the emission lines to discriminate between type 1 and 2 AGN. Here we follow an alternative approach. From the SDSS catalogues, we select the subset of SF (BPT classification = 1) and Seyfert AGN (BPT classification = 4) galaxies. In both sets, we measure the equivalent width of the $H\alpha$ line from the MPA/JHU catalogue, and define a simple proxy of the relative amplitude of the line with respect to the continuum, as follows:

$$A_{H\alpha} = \frac{\phi_{H\alpha}^{max} - \mathcal{C}_{H\alpha}}{\mathcal{C}_{H\alpha}}, \quad (2)$$

where $\phi_{H\alpha}^{max}$ and $\mathcal{C}_{H\alpha}$ denote the flux of emission and continuum at the location of the $H\alpha$ line ($\lambda = 6564.61\text{\AA}$ in vacuum), respectively. We divide the SF galaxies into different bins according to their $EW(H\alpha)$ and calculate the mean (μ_{SF}) and standard deviation (σ_{SF}) of the distribution of $A_{H\alpha}$ values. These estimates are used to differentiate between type 1 and 2, so that a Seyfert AGN galaxy is considered type 2 if, for a given $EW(H\alpha)$ its $A_{H\alpha}$ is located within $2\sigma_{SF}$ below the mean of the distribution of line amplitudes for the SF subset. This criterion results in 1,574 type 1 and 5,499 type 2 AGN galaxies – consistent with previous studies (Villarroel & Korn 2014). The second motivation for the use of $2\sigma_{SF}$ in the classification is more empirical, where we argue that for a given $EW(H\alpha)$, if the $A_{H\alpha}$ is too small, it must be due to the width of the line, i.e., corresponding to a type 1 AGN.

Fig. 1 illustrates this selection criterion. The blue, red and green data points show the distribution of SF, type 2

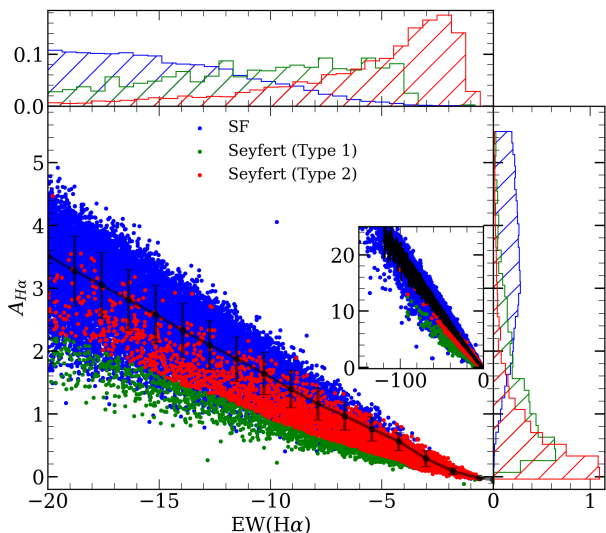


Figure 1. Distribution of star-forming and Seyfert galaxies from SDSS on the $A_{H\alpha}$ vs $EW(H\alpha)$ plane. The data points correspond to galaxies selected as type 1 AGN (green), type 2 AGN (red), or SF (blue). The central panel shows the region where most of the selected Seyfert galaxies are found, while the inset zooms out to show the overall distribution. The line and points with (1σ) error bars map the distribution of SF galaxies, used in the classification of type 1 vs type 2 AGN (see text for details). The top and right panels show the histograms of type 2, type 1 AGN, and SF galaxies in red, green and blue with respect to either $EW(H\alpha)$ or $A_{H\alpha}$.

and type 1 Seyfert galaxies, respectively. Note, while our method is a crude approximation, visual inspection of the spectra of individual galaxies confirms a low level incidence of broad line AGN galaxies in our type 2 definition. Additionally, Fig. A1 in Appendix A plots the stacked spectra of type 1 and 2 AGN galaxies, binned with respect to $EW(H\alpha)$, consistently showing that type 1 AGN have a broader $H\alpha$ line than type 2 AGN and SF galaxies. It is possible that this procedure still suffers from some level of cross contamination. However, due to the wide distribution of SF galaxies, it is most likely that the method falsely flags type 2 AGN as type 1. We argue this false classification will only lower the number of galaxy samples therefore leaving the stellar population properties, in general, unchanged.

3 STELLAR POPULATION DIFFERENCES

In this section, we study various properties of the twin galaxy sample from integrated spectra within three different circular apertures. Additionally, we test the robustness and the statistical significance of the results by comparing them with a larger, general sample from SDSS. The redshift range of the SDSS and CALIFA samples is slightly different, therefore a selection bias could be present in the comparison as: i) the two samples correspond to different cosmic time, and/or ii) we are affected by an aperture bias, as we observe different regions of the galaxies. We argue cosmic time is not a major issue as it does not vary significantly between

the different redshift ranges probed by the samples, $\lesssim 1$ Gyr. Regarding the latter, we assess the effect by producing CALIFA spectra within apertures that are equivalent to the area covered (in physical size) by the $3''$ diameter of the fibers of the original SDSS spectrograph.

3.1 Differences in the evolutionary stage of twin galaxies

In order to compare the evolutionary stage of twin galaxies, we adopt the $D_n(4000)$ -stellar mass plane in Figure 2 – instead of the standard colour-stellar mass diagram (Schawinski et al. 2014; Bremer et al. 2018). Each panel corresponds to a different twin. The blue, green and red filled regions depict the BC, GV and RS respectively; defined by the SDSS data (A19). The black filled circles, grey squares and unfilled circles show the result for measurements within three different apertures, namely $1.5''$, 2.2 kpc, and $1.5 R_{\text{eff}}$ (all defined by radius), respectively – Fig. C1 illustrates, for a single galaxy, the aforementioned apertures. The first one ($R \leq 1.5''$) concerns the data from the innermost region of the galaxies, thus studying the immediate vicinity where the AGN has the highest impact. It also takes into account the smearing of the point spread function. The $R \leq 2.2$ kpc is justified for a comparison between SDSS data and this sample, by matching the aperture size to the physical extent of the SDSS fibre at the median SDSS redshift ($z \sim 0.077$). Note the median redshift for the CALIFA survey is $z \sim 0.015$. The last aperture ($1.5 R_{\text{eff}}$) is meant to explore most of the galaxy, within the reach of the CALIFA survey. Note the $D_n(4000)$ measurements are carried out on spectra that have been smoothed to a common velocity dispersion, ~ 220 km/s (i.e. approximately the maximum value in the sample). In each twin, the AGN galaxy is shown in black, while the SF counterpart(s) are shown in blue, green or red. The strongest trend in this sample shows that 9 out of 10 twin pairs have an AGN with a greater 4000\AA break than their SF counterparts, even amongst twin samples, in both their central regions ($1.5''$), and within 2.2 kpc, indicating the importance of AGN in quenching star formation (Schawinski et al. 2007; Bell 2008). The case for a 2.2 kpc aperture – defined to match results with SDSS spectra – shows that most AGN galaxies, $\sim 71\%$, reside in the GV. Here we have identified galaxies as residing in GV, even if they are slightly above BC or below RS; this is based on how we define GV galaxies in A19 and A20. Previous work from the literature based on SDSS, MaNGA and CALIFA data have also noted that a high fraction of AGN, specifically LINER galaxies occupy the GV (Martin et al. 2007; Sánchez et al. 2018; Anghop et al. 2019; Lacerda et al. 2020). In addition, both AGN and SF galaxies show a decrease in 4000\AA break strength radially outward, thus indicating older stellar populations in the centre, suggestive of inside-out quenching (Kelvin et al. 2018). The only exception to this trend is seen in the 3 SF galaxies belonging to twin 1 and twin 5, where the stellar populations within 2.2 kpc have a greater $D_n(4000)$ index than those within $1.5''$. All 4 SF galaxies are barred spiral galaxies, indicating younger stellar populations at the most central region. Note, del Moral-Castro et al. (2019) also found similar results in the pilot study regarding twin galaxies.

Using the aperture of the most central region, i.e. $1.5''$, the twin(s) are binned into different groups (as labelled in

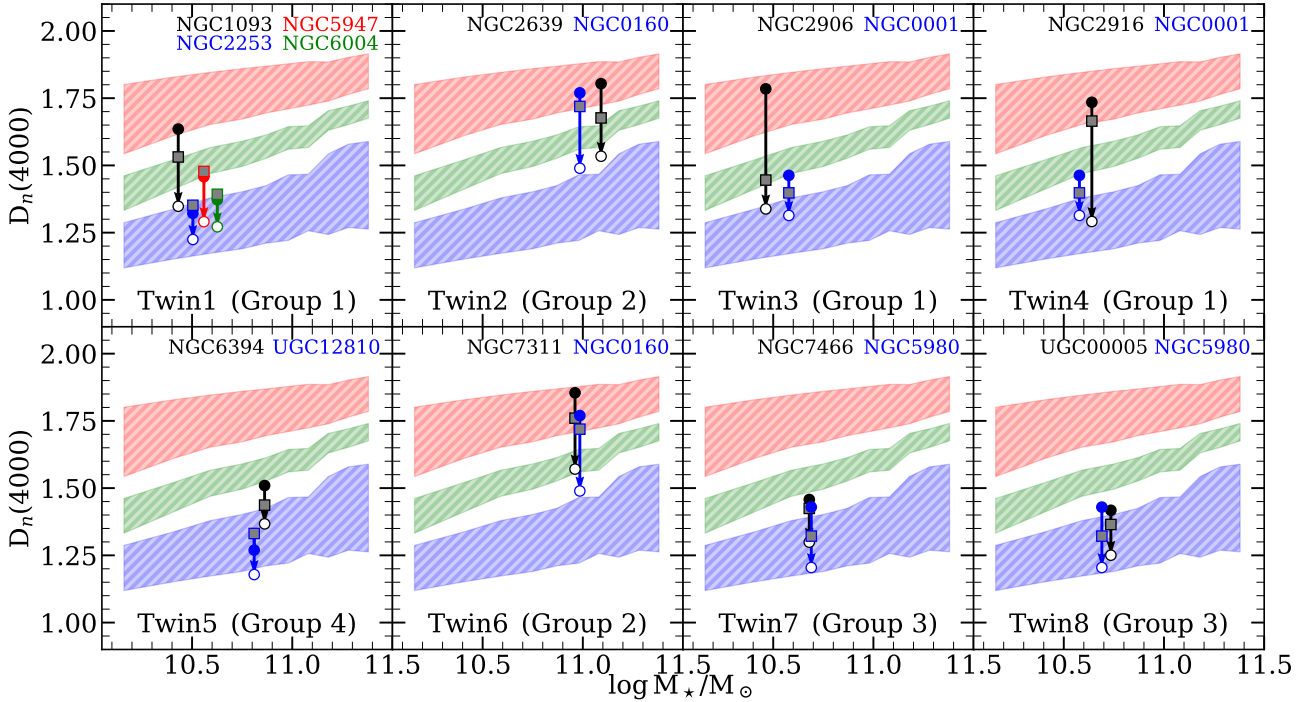


Figure 2. Distribution of twin galaxies on the $D_n(4000)$ vs stellar mass plane. The blue, green and red filled regions respectively map the BC, GV and RS defined in A19 and A20. Each panel shows the twin galaxy pairs, where the black circles are the AGN-hosting galaxies, and the coloured circles represent the non-AGN (i.e. SF) counterparts, all measured within a $1.5''$ aperture, similar to the PSF of CALIFA. The grey squares are the results within a 2.2 kpc aperture radii, and the white circles correspond to the largest aperture in this study, $R \leq 1.5R_{\text{eff}}$. Note, the error on $D_n(4000)$ is calculated via Monte Carlo realisation, where due to high SNR on the spectra, uncertainties on measurements of the index is minuscule, $\Delta D_n(4000) \leq 0.01$. From the original twin sample of 11 systems (10 Type 2 Seyfert AGN and 1 Type 1 Seyfert AGN), we reject three (see text for details) pairs.

Fig. 2), based on their location in the diagram. Group 1 (G1) consists of twins 1, 3 and 4, as their AGN galaxy resides in the RS, whereas their SF galaxies reside in either the BC or GV. Group 2 (G2) consists of twins 2 and 6, since both their AGN and SF galaxies are in the RS. Group 3 (G3) is made up of twins 7 and 8, as both AGN and SF galaxies reside in the GV/BC region. Finally, twin 5 alone is grouped in G4 as this is the only twin with the AGN galaxy in the GV, whereas its SF counterpart is clearly in the BC. The grouping is robust as it does not depend significantly on the adopted aperture. Using the $R \leq 2.2$ kpc spectra to define the groups, we find $\sim 22\%$ of the grouping would change, as twin 4 would be on its own group and twin 5 would join twins 7 and 8. Similarly, using the $1.5R_{\text{eff}}$ aperture, the grouping structure would remain the same, but twins 5, 7 and 8 would be put together.

From these groups, we aim to test whether variations in stellar properties are caused either by the presence of an AGN, or by the galaxies being at different stages of evolution. It is evident for G1 that AGN galaxies are more evolved than SF galaxies within $1.5''$. Note that while the $D_n(4000)$ vs stellar mass diagram is a proxy of evolution, as galaxies are expected to transition from the BC to RS via the GV, the actual path could be complicated by rejuvenation events (Thomas et al. 2010). We argue that rejuvenation should not play an important role in our sample as (i) these galax-

ies are selected to be isolated, therefore it is unlikely they have undergone major merging event. However recent minor mergers cannot be ruled out and (ii) state-of-the-art simulations, IllustrisTNG, have noted that rejuvenation events are more prominent at high stellar mass $\gtrsim 10^{11} M_{\odot}$ (Nelson et al. 2018), thus above the mass range probed by this sample.

3.2 Contrasting with the general galaxy population (SDSS)

Fig. 2 therefore suggests that AGN galaxies tend to be more evolved compared to their twin SF counterparts. Previous work noted this trend as well, where a high fraction of AGN galaxies is found in the GV (Sánchez et al. 2018; Lacerda et al. 2020), whereas most of the SF galaxies are located in the BC. However, our result is more focused, as it targets sets of carefully defined pairs with very similar overall properties except for the presence of an AGN. Owing to the small sample size, we address now the statistical significance of our results, by comparing the sample with a large, general distribution of galaxies from the SDSS.

3.2.1 Line strengths

The differences found in Fig. 2 are still open to a potential sample selection effect. We need to assess whether the popu-

lation properties of the twin galaxies is comparable with the general sample, i.e. are these galaxies a fair representation of their counterparts in SDSS, or are they statistical outliers? We compare key line strengths, $D_n(4000)$, $H\delta_A$ and $[MgFe]'$ within the 2.2 kpc aperture with respect to the distribution of galaxies in SDSS. We select spiral galaxies from SDSS, making use of the Galaxy Zoo catalogue (Lintott et al. 2008), choosing the spiral flag set to 1. Additionally, we do not smooth the spectra of the twin galaxies to $\sigma \sim 220$ km/s, unlike in previous and future sections, as the SDSS spectra are not smoothed either. Note, the smoothing has a small effect on the line strength, where we find the largest differences for $[MgFe]'$, with a maximum offset of ~ 0.26 dex. Fig. 3 shows the distribution of 4000Å break strength for each twin – where the SDSS sample is restricted to the same stellar mass, within $\Delta \log M_*/M_\odot = \pm 0.2$ dex. The vertical dashed lines locate the $D_n(4000)$ index for the twin galaxies: black for the AGN, coloured lines for SF systems. The solid blue and grey histograms show the distribution of SDSS galaxies classified as SF and type 2 Seyfert, respectively.

In G1, both twins 1 and 3 show the AGN galaxies close to the peak of the type 2 AGN distribution. In contrast, the AGN galaxy of twin 4 is offset with respect to the peak of the Seyfert distribution, by $\gtrsim 1\sigma$. SF galaxies in all 3 twins belonging to group 1 are more representative of the general sample, and are located towards the peak of the SDSS SF galaxy distribution. Note, while the corresponding histogram for the complete sample is not shown it also peaks at the same location as the "SF" sample, indicating a high absolute number of SF galaxies within the chosen stellar mass. SF galaxies in G2 are located near the tail end of the SDSS SF galaxy distribution, whereas the AGN are neighbouring the peak of SDSS type 2 Seyfert distribution. Thus, while possible, such twin pairings are unlikely if extracted randomly from a larger, general sample. G3 and G4 show similar trends, to that of G1, where the 4000Å break of the AGN is located close to peak of Seyferts. For each twin, the SF galaxies tend to have their 4000Å break close to the peak of the SDSS SF distribution. Therefore, if we were to extend the sample to a larger survey, we would find that twins 1, 3, 4, 5, 7 and 8 are representative samples of the general population.

Fig. 4 and Fig. 5 show the $H\delta_A$ and $[MgFe]'$ distribution for AGN and SF galaxies, with the colour-coded vertical lines once more representing the individual measurements of galaxies in the twin samples. The SDSS distributions follow the same labelling system as Fig. 3. All twins in G1 have $H\delta_A$ for AGN and SF galaxies compatible with respect to the SDSS distribution, with the exception of NGC5947 in twin 1. Similarly to $D_n(4000)$, the $H\delta_A$ strength of SF galaxies in G2 are at the tail end of the distribution, while AGN galaxies are located closer to the peak of type 2 Seyfert AGN. G3 and G4 suggest a high likelihood of finding both AGN and SF galaxies with the observed $H\delta_A$, with the exception of twin 7 where the AGN is located $\gtrsim 1\sigma$ away from the peak of the distribution. For G1, G3 and G4, the $[MgFe]'$ index in both AGN and SF galaxies resembles that of the larger SDSS sample, once more with the exception of NGC5947. In comparison, G2 shows the twin SF galaxy to deviate away from the peak location by $\gtrsim 1\sigma$, whereas the AGN galaxies appear closer to the peak of the distribution in type 2 Seyfert systems. The inclusion of $H\delta_A$ and $[MgFe]'$ shows, given their

position in the evolutionary sequence, how alike the twin galaxies are to a larger parent sample.

3.2.2 Testing the significance of the relative differences

We focus here on one key question: how significant is the difference found in the $D_n(4000)$ vs stellar mass plane between the twin pairs, with respect to a random pairing of galaxies with similar mass? To answer this, we look at the relative difference in 4000Å break strength between the twin samples, measured within a 2.2 kpc aperture, and compare it with random pairings of galaxies with similar stellar mass (within $\Delta \log M_*/M_\odot = \pm 0.2$ dex) from SDSS. We define the relative difference as follows:

$$\delta(\Psi) = \frac{\Psi_1 - \Psi_2}{\Psi_1}, \quad (3)$$

where Ψ_1 and Ψ_2 are the line strengths of the galaxies in each pair.

Fig. 6 shows as vertical lines the observed relative difference in the twin sample, where the blue, red, green and orange lines show differences for individual twins, as labelled, while the black vertical line shows the average of the four twins. Note twin 1 has multiple pairs comprising 1 AGN and 3 SF galaxies, therefore we show the average of the three pairs. The SDSS data are represented as a Gaussian distribution (i.e. taking the mean and standard deviation of the SDSS sample to produce a Gaussian equivalent). The blue distribution shows the result when selecting random pairs from the subset of only SF galaxies, in SDSS and the grey distribution corresponds to random pairings that include SF and type 2 Seyfert AGN galaxies. Note these pairings can be SF-SF, SF-AGN or AGN-AGN. The figure is split according to stellar mass, where the left panel shows differences for SDSS galaxies within $10.28 \lesssim \log M_*/M_\odot \lesssim 10.78$ and the right panel shows differences within $10.66 \lesssim \log M_*/M_\odot \lesssim 11.16$. We find all twins (except twin 4) to have relative differences within 1σ (2σ) of the SDSS relative difference distribution for both SF and AGN galaxies. Note, while the variation seems to be statistically small, the relative difference is generally positive, suggesting the results found in Fig. 6 indicate physical differences between the evolutionary stage of twin galaxies, so that galaxies hosting an AGN have stronger 4000Å break strengths than their SF counterparts - even when considering "twin" galaxies. This paper relies on a rather small set of twin galaxies as a proof of concept. Future studies, with larger data sets, will allow us to produce more conclusive results. However, the present sample already shows the high diversity in twin pairs, which rules out simple AGN feedback models.

3.3 Inner vs Outer regions

We consider now the difference in line strength between the smallest aperture, $1.5''$, and the largest one, extending to $1.5 R_{\text{eff}}$, by comparing the age-sensitive indices, $D_n(4000)$ and $H\delta_A$, as well as the metallicity-sensitive index, $[MgFe]'$. We define the absolute difference between line strengths with respect to aperture as:

$$\Delta\Psi = \Psi(R \leq 1.5'') - \Psi(R \leq 1.5R_{\text{eff}}), \quad (4)$$

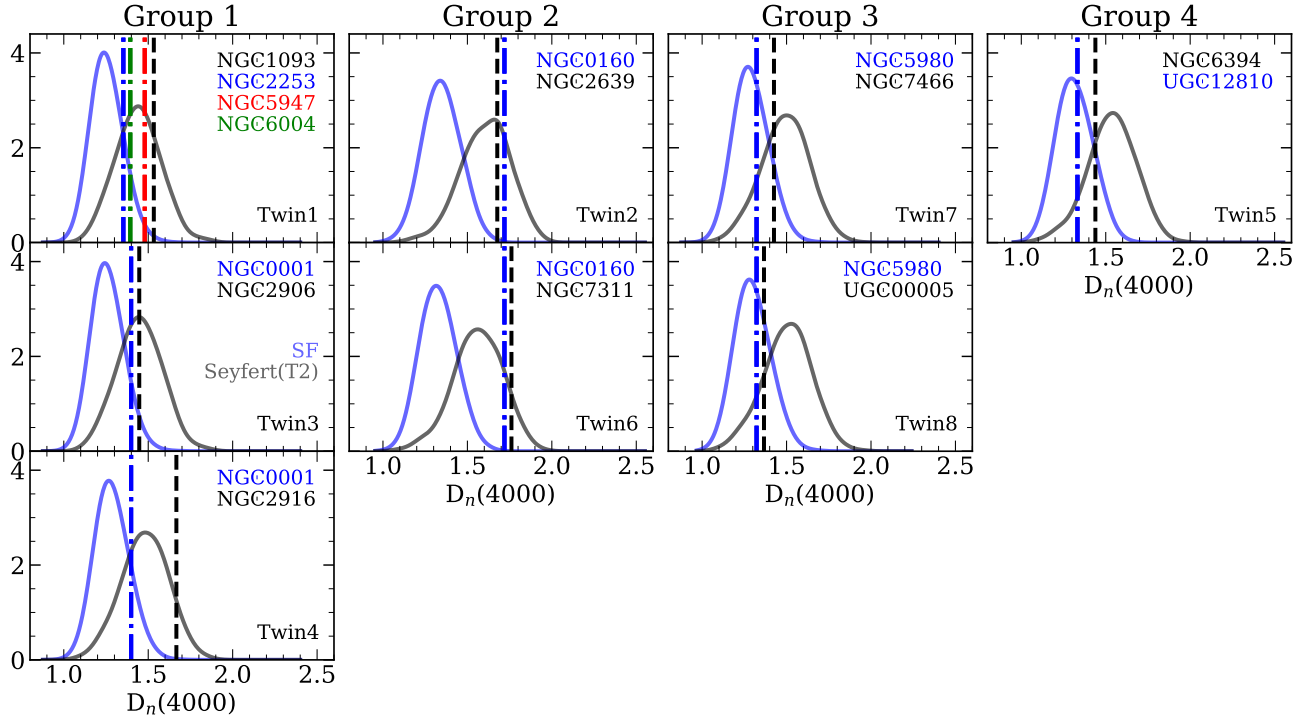


Figure 3. General distribution of $D_n(4000)$. The blue and grey Kernel Density Estimation (KDE) histograms show the distribution of star-forming and type 2 Seyfert AGN from a sample of SDSS within a range of stellar mass compatible for each twin. The black dashed vertical line shows the $D_n(4000)$ index for the AGN in the twins, while the dash-dotted lines, with varying colours, show the $D_n(4000)$ index for SF twins. The twin estimates are given for a 2.2kpc aperture to match the SDSS sample. See text for details.

where Ψ represents the different indices – either $D_n(4000)$, $H\delta_A$ or $[\text{MgFe}]'$.

3.3.1 Age Sensitive Indices

Fig. 7 shows $\Delta D_n(4000)$ vs $\Delta H\delta_A$ for galaxies split in panels with respect to the four groups. The different colours denote different twins, as labelled. AGN galaxies are indicated by a circular data point, whereas SF galaxies are shown by a cross. G1 galaxies – i.e. twins 1, 3 and 4 in the top-left panel, show a clean trend where galaxies hosting the AGN have a greater difference between the central and outer regions in both indices. AGN galaxies have a difference of $\Delta D_n(4000) \gtrsim 0.2$ and $\Delta H\delta_A \lesssim -2.6$. Both AGN and SF galaxies feature an older central part compared to the outer regions, favouring the idea of inside-out quenching (e.g. Spindler et al. 2018; Kelvin et al. 2018). In G2, twins 3 and 4, the $1.5 R_{\text{eff}}$ aperture spectra show similar 4000\AA break, regardless of galaxy type (see Fig. 2). In contrast, the SF systems have a consistently lower difference between central and outer apertures $\Delta D_n(4000) \lesssim 0.2$ and $\Delta H\delta_A \gtrsim -2.6$, indicating that the presence of an AGN preferentially quenches the central region. The G4 twins (bottom-right panel) show a similar trend, where the radial difference in 4000\AA break strength is greater in the AGN system, although the difference here is more subtle. Note that G4 is defined by a twin where the AGN is in the “lower” part of the GV and the SF is in the BC. This figure shows

that, in addition, the radial trends are shallower, and less distinguishable between AGN and SF galaxies.

G2 galaxies show substantial gradients, once more suggesting older populations in the central regions. However, there is no clear difference between AGN and SF members, a result that could be expected from the fact that G2 twins *both* have the central spectra in the RS, and the $1.5 R_{\text{eff}}$ spectra in the upper portion of the BC. We can thus assume that the SF galaxy, while being classified as SF, is a system closer to end of its star formation cycle. This is further supported by their earlier disc morphological classification (Sa). In a general context, group G2 is an anomaly in our sample. In G3 both AGN and SF galaxies reside in the lower part of the GV. Here, a substantial difference is found in the radial gradient of 4000\AA break strength, with larger variations in the SF systems with respect to the AGN, whereas $H\delta_A$ has similar variations within this group.

3.3.2 Metallicity Sensitive Indices

Fig. 8 shows the equivalent of Fig. 7, replacing $H\delta_A$ with the metallicity-sensitive index $[\text{MgFe}]'$, following the same labelling and colour coding. Once more, G1 galaxies show the clearest trend, where AGN systems have a greater difference in $[\text{MgFe}]'$ ($\Delta[\text{MgFe}]' \gtrsim 0.6$), with respect to their SF twin counterpart ($\Delta[\text{MgFe}]' \lesssim 0.5$). This trend suggests a more metal rich population in the central regions regardless of galaxy type, as $\Delta[\text{MgFe}]' \gtrsim 0$, however, the AGN consis-

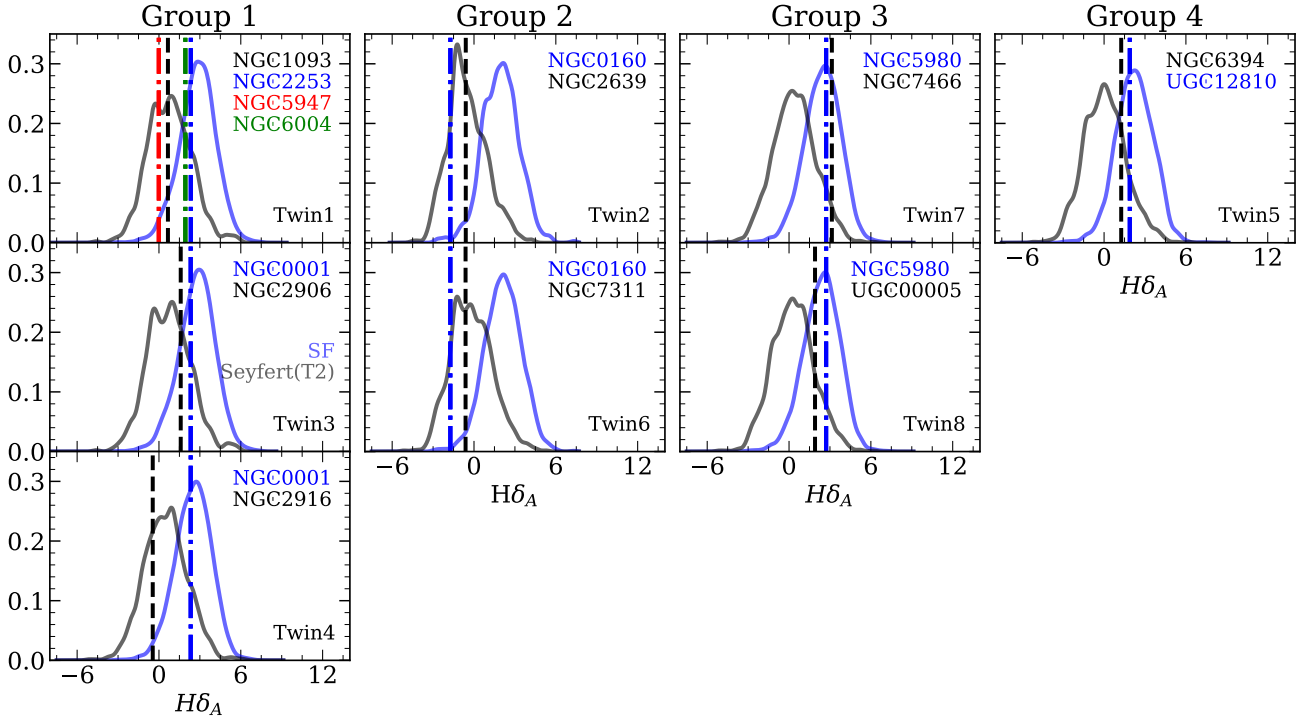


Figure 4. Same as Fig. 3 for the distribution of $H\delta_A$ line strengths.

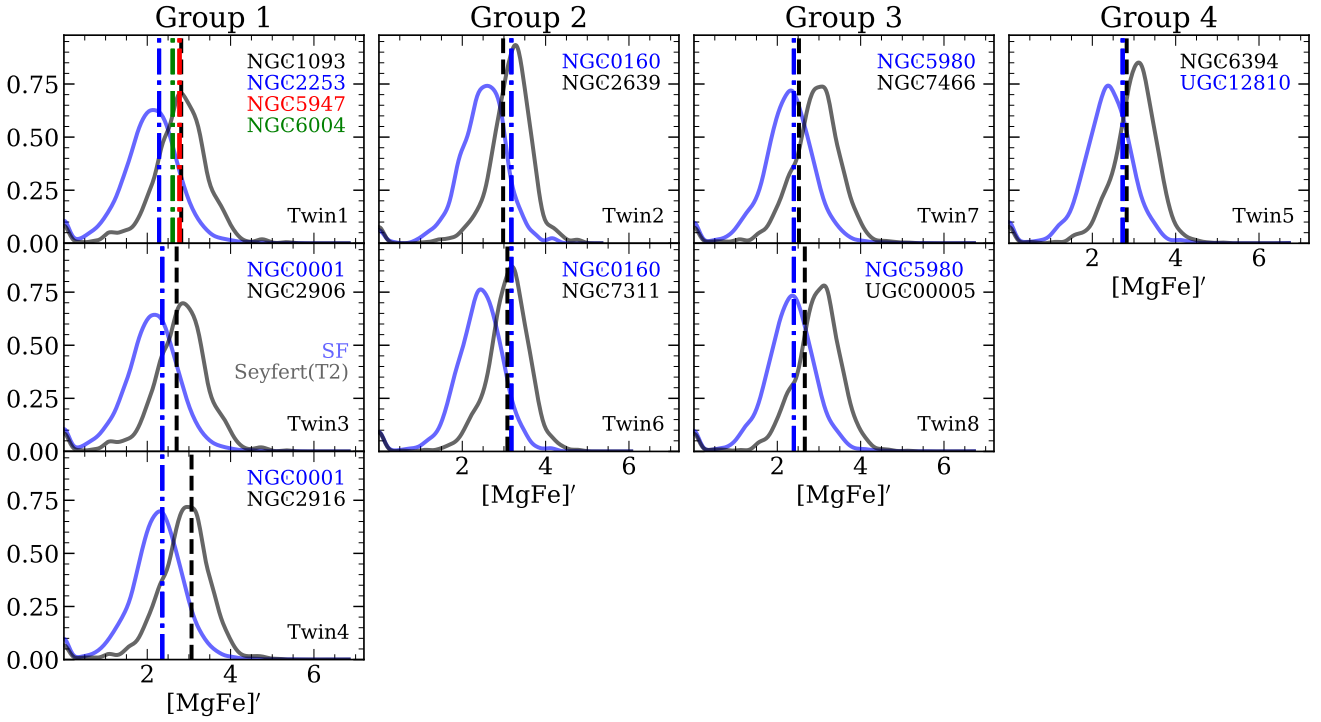


Figure 5. Same as Fig. 3 for the distribution of $[MgFe]'$ line strengths.

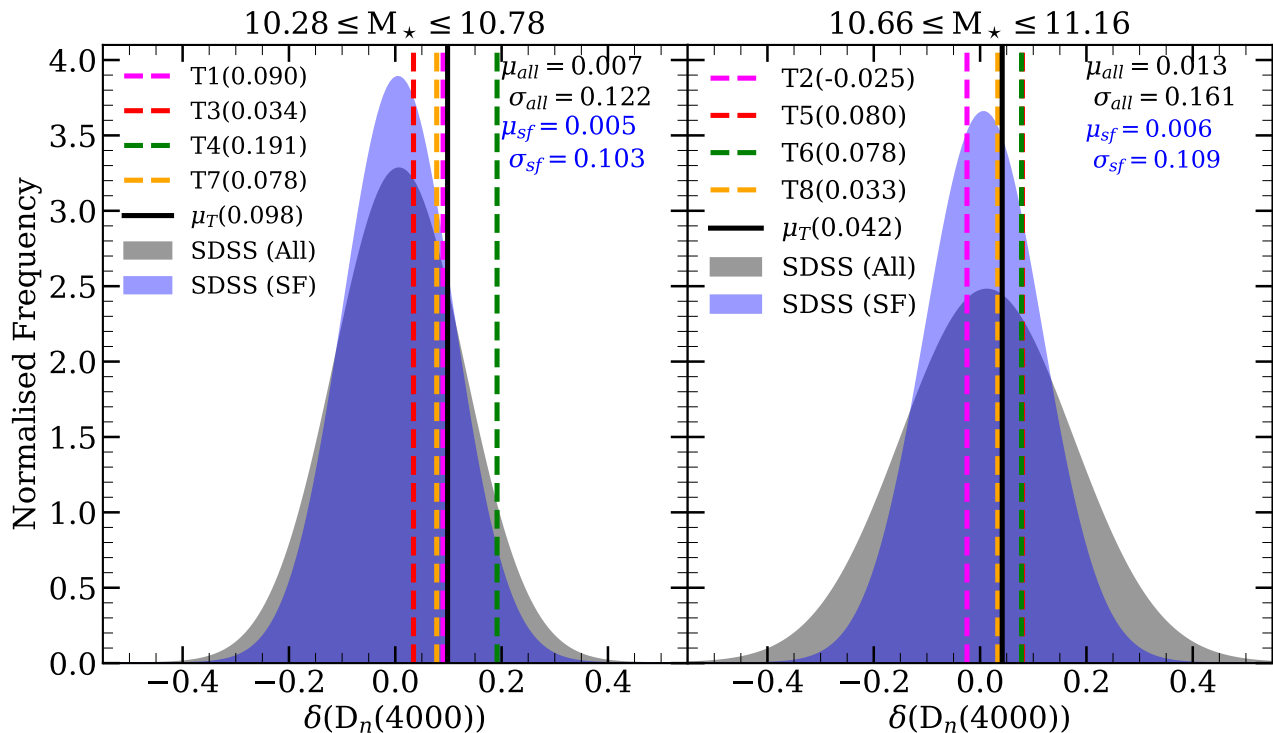


Figure 6. The significance of the results is tested with the relative difference of the $D_n(4000)$ index between galaxies in each twin pair, contrasted with random samples from SDSS (assuming Gaussian distributions). The blue distribution corresponds to random pairs of star-forming galaxies in SDSS. The grey distribution corresponds to random sets where both star-forming and type 2 Seyfert AGN from SDSS are considered. The panels are split with respect to the stellar mass, $10.28 \lesssim \log M_*/M_\odot \lesssim 10.78$ (left) and $10.66 \lesssim \log M_*/M_\odot \lesssim 11.16$ (right). The vertical lines mark the observed relative differences in the twin pairs, as labelled.

tently have higher gradients. G3 and G4 galaxies show no clear difference between AGN and SF galaxies, given the error bars, but they consistently feature negative radial gradients in metallicity ($\Delta[\text{MgFe}]' \gtrsim 0.25$). A slightly more significant trend is shown in G2, where in both twins, SF galaxies have a greater difference between apertures, $\Delta[\text{MgFe}]' \gtrsim 0.8$, compared to their AGN counterpart $\Delta[\text{MgFe}]' \lesssim 0.8$. Note, there are large uncertainties associated to the data points.

These results suggest an alternate view of the radial extent of AGN feedback. If we were to believe low-to-intermediate AGN activity only affects the formation history within a relatively small region around the centre, we should consistently find greater differences in the AGN galaxy of each twin. The data are not conclusive, and reveals mixed distributions. Furthermore, del Moral-Castro et al. (in prep.) will investigate these results further using spectral fitting. The implications of this are discussed in Sec. 4.

3.4 SSP Parameters

In this section, the SSP equivalent ages and metallicities are estimated for the twin galaxies within the 3 different apertures. We make use of the MIUSCAT population synthesis models (Vazdekis et al. 2012), constructing a grid consisting of 8192 synthetic spectra, 128 ages varying from 0.1 to 13.5 Gyr in a logarithmic scale. Similarly, the metallicity

varies from $[Z/H] = -2.0$ to $+0.2$ also in log steps. The best fit to the SSPs adopts a χ^2 statistic defined as follows:

$$\chi^2(t, Z) = \sum_i \left[\frac{\Delta_i(t, Z)}{\sigma_i} \right]^2, \quad (5)$$

where $\Delta_i(t, Z) = O_i - M_i(t, Z) - \delta_i$ is the difference between the observed and model index with an offset (δ_i) for the i th index. This offset is introduced due to the high S/N in our observed spectra, at a level where the SSP models are not capable of fully reproducing all the details. The uncertainties $\sigma_i = \sqrt{\sigma_{i, err}^2 + (0.05 O_i)^2}$, encapsulate both the statistical error in the index along with an extra term amounting to 5% of the index value. This way we account for both the systematics associated with our methodology and include a conservative uncertainty in our calculations. The χ^2 statistic involves a set of seven different spectral indices: $D_n(4000)$, $H\delta_A$ and $H\gamma_A$ (age sensitive indices), and Mgb , $\text{Fe}5270$, $\text{Fe}5335$ and $[\text{MgFe}]'$ (metallicity sensitive indices). The likelihood corresponding to the SSP-equivalent estimates of age and metallicity are obtained by marginalising over the unwanted parameter. While some indices are described as ‘‘age-sensitive’’ and others are ‘‘metallicity-sensitive’’, all of the indices suffer from the age-metallicity degeneracy (Worthey 1994).

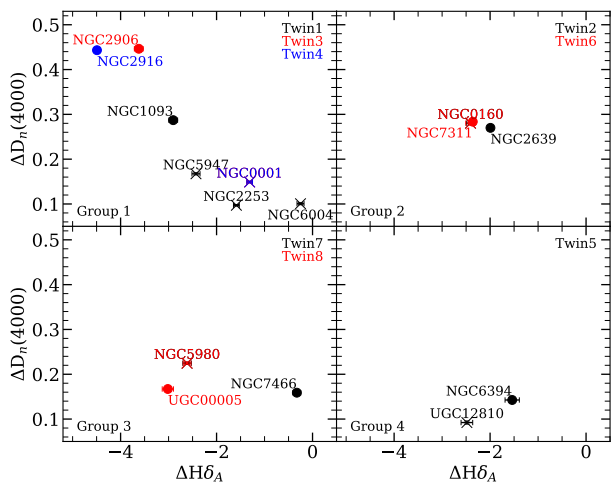


Figure 7. Line strength difference between the central region ($1.5''$) and the largest aperture ($1.5 R_{\text{eff}}$), regarding $H\delta_A$ and $D_n(4000)$. The circular data points denote galaxies hosting an AGN, whereas the cross symbol shows the SF counterparts. Each colour identifies twins, as labelled in each panel. Note that some twins have the same SF galaxy (NGC0160, NGC0001 and NGC5980), so those appear repeated in the figure, hence they have overlapping data points. The uncertainties are produced with a set of Monte Carlo realisations.

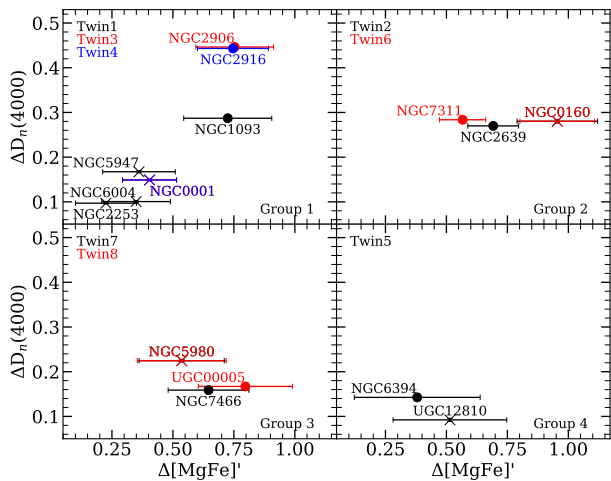


Figure 8. Same as Fig. 7, showing a line strength diagram comprising $D_n(4000)$ vs $[MgFe]'$.

3.4.1 Age parameters

Fig. 9 shows the SSP equivalent age for different groups within different apertures. The left, middle and right panels show the ages for the central $1.5''$, 2.2 kpc and $1.5 R_{\text{eff}}$ apertures, respectively. The black data points show the ages of the AGN galaxy in each twin, while the other colours represent the ages of SF galaxies. Circle, square, pentagon and triangle symbols denote G1, G2, G3 and G4, respectively. We find 80%, 40% and 60% of the AGN galaxies in the twin being equal or older than their SF counterpart for

G1 galaxies inside of the $1.5''$, 2.2 kpc and $1.5 R_{\text{eff}}$ apertures, respectively. In G2, AGN galaxies have equal or younger average ages compared to their SF counterpart 83% of the time, even though in the evolutionary sequence, within a $1.5''$ aperture, we find these AGN to have a stronger 4000\AA break. G3 twins show no clear trend in the inner regions ($1.5''$ and 2.2 kpc) but show older populations in AGN with respect to SF galaxies, for both twins, in the $1.5 R_{\text{eff}}$ aperture. G4 follows the opposite trend, where the AGN galaxy is older within both $1.5''$ and 2.2 kpc apertures, but is younger, than the SF galaxy, when considering the largest aperture.

If we consider all the twins in the different groups, in all apertures, we find that 50% of twins show equal or older populations in the AGN galaxies (70% in $1.5''$, 30% within 2.2 kpc and 50% for the largest aperture). This indicates that the AGN exerts the most impact within the most central region of the galaxy.

3.4.2 Metallicity parameters

Fig. 10 shows the SSP-equivalent metallicities, from left to right, within the central $1.5''$, 2.2 kpc , and $1.5 R_{\text{eff}}$ apertures, respectively. The symbols and colours are equivalent to those shown in Fig. 9. Similarly to the age estimates, within $1.5''$, G1 galaxies have AGN that are more metal rich than the SF galaxies 80% of the time. G2 and G3 show no clear trend. Finally G4, also shows AGN galaxies to be more metal rich. In the 2.2 kpc aperture G1 and G3 host AGN galaxies that are equal or more metal rich than their SF counterpart 100% of the times. G4 shows the SF galaxy to be more metal rich, however the differences are within 1σ . For the more metal rich AGN galaxies, we sometimes find them to be younger than their SF counterpart, perhaps a sign of the age-metallicity degeneracy. However in Appendix B, we show the bivariate confidence levels in age and metallicity for 2 twins, rejecting a substantial bias from this degeneracy, specifically for twins where we find the AGN galaxy to be more metal rich. Therefore, at least within a 2.2 kpc aperture, the metallicity trend indicates that the presence of an AGN is potentially related to a different star formation history, with respect to the SF counterpart. This is further backed up by the spectra in the largest aperture, $1.5 R_{\text{eff}}$ trends, where we find that the AGN galaxies in G1 and G4 are more metal rich compared to their SF counterpart. Note, while we find strong evidence showing AGN galaxies are likely to be more metal rich, some twins show large overlap between AGN and SF twins. Furthermore, rather than looking at an individual group within a fixed aperture, if we look at all the different groups and in all apertures, we find AGN galaxies to be more metal rich 73% of the time compared to their SF counterparts. Breaking this into different apertures, we find 70%, 80% and 70% of AGN galaxies to be more metal rich in the $1.5''$, 2.2 kpc , and $1.5 R_{\text{eff}}$, respectively. Note, some of these galaxies have values, which are compatible within 1σ .

4 DISCUSSION

This paper explores the transitional role of AGN activity by analysing pairs of galaxies defined as twins, inasmuch as they feature similar large galaxy-scale properties but one

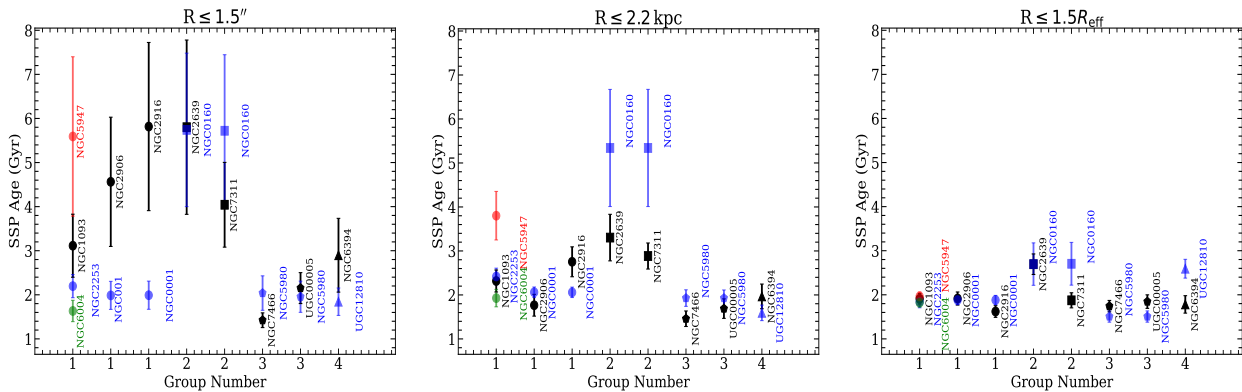


Figure 9. SSP equivalent average ages for twin galaxies in different groups. The black and coloured data points, blue, green and red, show the results for AGN and non-AGN galaxies, respectively. The error bars are given at the 1σ confidence level, obtained by calculating the normalised likelihood value, which makes use of the different χ^2 values. The error on each of the individual line strengths are obtained by making 100 Monte Carlo realisations of the spectra - which is used to calculate the χ^2 with best fit. From left to right, we show the results for twins 1, 3, 4, 2, 6, 7, 8, and 5. Furthermore, the circle, square, pentagon and triangle symbols identify groups 1, 2, 3 and 4, respectively.

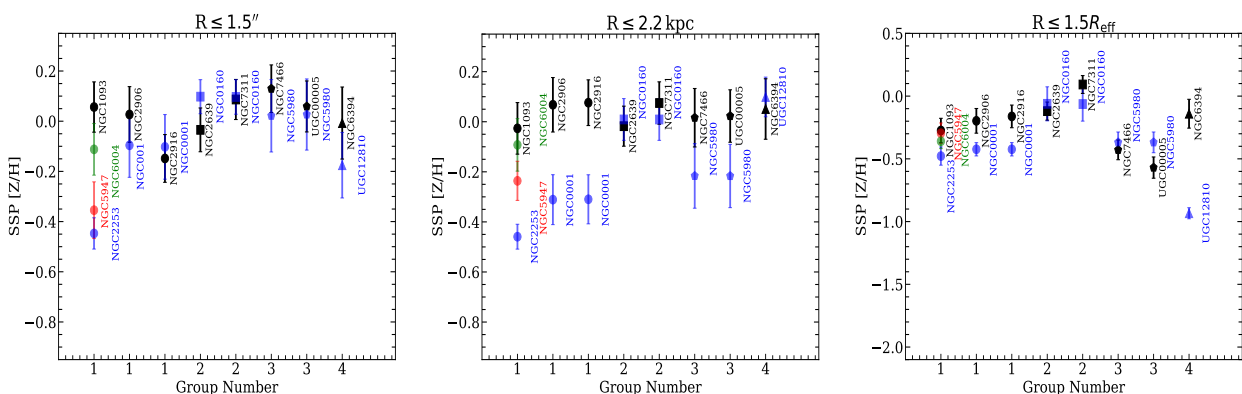


Figure 10. Same as Fig. 9 for the SSP equivalent metallicity of the twin pairs, following an identical notation.

presents AGN activity and the other one does not. The definition of these twin pairs follows the methodology laid out in [del Moral-Castro et al. \(2020\)](#). In this section we discuss the potential implications of our results, from the radial influence of AGN activity on the galaxy, to testing two alternative hypotheses, either an “on-off” AGN switching mode, or the possibility of the twins having different evolutionary paths. Owing to the small sample size (10 twins comprising 8 AGN and 7 SF galaxies due to some AGN galaxies have multiple SF pairs), we mostly find mixed trends in the behaviour of the individual twins. A key reason for such difference could be due to their differing location on the evolutionary sequence, as galaxies on the BC have different stellar populations with respect to those on the GV or RS. Nevertheless, a statistical comparison of the CALIFA spectra measured within 2.2 kpc with respect to a more general sample from SDSS suggests that many of these twins – twin pair 1, 3, 4, 5, 7 and 8 – are representative of the larger sample, taken from SDSS (see Figs. 3, 4, and 5), thus providing strong motivation for similar studies in larger data sets.

4.1 Potential Caveats

This paper is meant to present a methodological approach that can be used to assess the role of AGN in quenching star formation in galaxies, focusing on the diagram that presents the transition Blue Cloud/Green Valley/Red Sequence as a fundamental evolutionary sequence (Fig. 2). While larger data sets are needed to draw strong conclusions, this paper illustrates how this type of information can be retrieved from a reduced sample of twin pairs. We discuss here some of the caveats one should be aware of.

Note for the selection of the AGN and SF galaxies, we use the BPT classification scheme ([Baldwin et al. 1981](#)). The analysis is applied to the central spaxel of each galaxy. This could introduce a systematic trend, as the separation between AGN and SF activity on the BPT diagram mainly depends on the hardness of the radiation field, whereas other parameters, such as metallicity, pressure, the ionisation parameter, or the presence of shocks, will also affect the emission lines adopted in this classification ([Kewley et al. 2019](#)). Furthermore, previous studies have found the SF region of the BPT diagnostic diagram to be systematically metal

poorer than in the AGN region (Kewley et al. 2013; Ji et al. 2020). In this work, the AGN classification is based on the central spaxel, with an effective resolution of $1''$, whereas our analysis of line strengths and SSP age and metallicity are carried out in radii of $1.5''$, 2.2 kpc, and $1.5 R_{\text{eff}}$.

Another caveat is the small sample size of our data; we have only 8 different AGN galaxies and 7 SF galaxies. Throughout our study we have assumed that G1 and G4 galaxies are to be most representative of the larger sample, as these galaxies have $D_n(4000)$, $H\delta_A$ and $[\text{MgFe}]'$ values located at the peak of their respective SDSS galaxy distribution. This suggests that if we were to carry out a study on a larger sample, we would expect many of the twin pairings to be similar to those belonging to G1 and G4. However, this is inconclusive due to our statistically small sample. While G2 and G3 twins have SF galaxies located away from the peak of the SDSS galaxy distribution, a larger study might find G2 and G3 to be more representative of “twin” samples. This could be owing to most SF galaxies not being representative of the “twin” control sample of AGN galaxies. However, the key result from such grouping should be their diversity even amongst “twins”, indicating the effect of AGN on the stellar population of their host to be of a complex nature. Such diverse grouping motivates the need for a larger study.

4.2 Radial population variation

Both AGN and SF galaxies present mostly older stellar populations in the inner part of the galaxy, with a decreasing gradient as we move radially out (Sec. 3), in agreement with del Moral-Castro et al. (in prep.), who adopt a full spectral fitting approach. Sánchez et al. (2018) also find similar results in the MaNGA survey, using the derived star formation rate and gas density of their sample. Similarly, studies of stellar populations at different radii in CALIFA unveil similar trends, noting a decrease in age and metallicity for different types of galaxies at increasing radii (Bitsakis et al. 2019; Lacerna et al. 2020; Kalinova et al. 2021). All three results favour inside-out quenching (Lipari et al. 1994; Tacchella et al. 2015; Li et al. 2015; Breda et al. 2020), which suggests a galaxy may run out of gas without any interaction with other galaxies, involving internal processes, for instance, through secular evolution.

4.3 “On-off” AGN hypothesis

The next two subsections propose the interpretation of the results with two alternative scenarios. While the sample size in this work is rather small, preventing us from producing strong conclusions, these simple scenarios can be adopted to larger samples, to assess the role of AGN in quenching star formation.

The first one invokes a simple “on-off” AGN mode to explain the results. This scenario is motivated by the fact that most galaxies experience AGN events but some happen to be in an active phase (“on” state), while others are dormant (“off” state). The timescale of individual “on-off” events is expected to be around $\sim 10^5$ yr, where the whole life cycle lasts for $\sim 10^7 - 10^9$ yr (see, e.g., Schawinski et al. 2015). In such a cyclic behaviour, it is possible to explain the similarities and differences in twin pairs. Fig. 11 illustrates

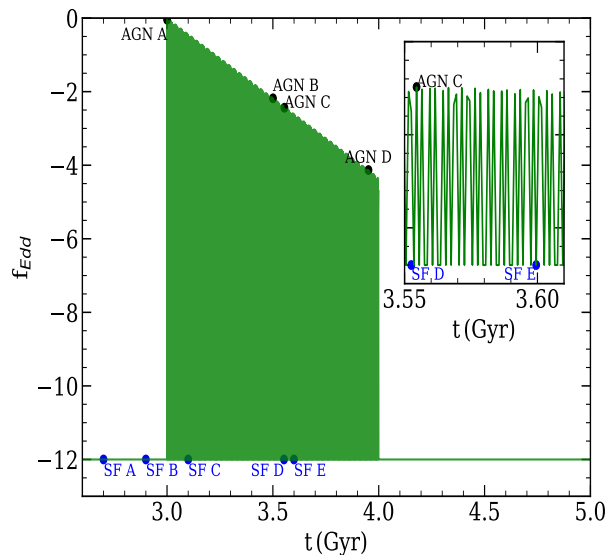


Figure 11. The fluctuating activity of the AGN in a galaxy is illustrated by this simple schematic that plots the evolution of the Eddington ratio of the SMBH (f_{Edd}), in green, throughout a galaxy’s life cycle. The dots give examples of galaxies that will be identified as AGN (black) or SF (blue) when classified on the BPT diagram, respectively. In the “on-off” model, the behaviour in f_{Edd} will rapidly quench star formation when the AGN is in an “on” mode (high f_{Edd}), at least within the central region, resuming the star formation activity once it goes back to the “off” mode (low f_{Edd}) - depending on whether enough gas available for star formation is left over. This “on-off” behaviour operates over timescales that are much shorter than the sensitivity of line strengths, and even emission lines (from the ionising photons of massive stars). Therefore, we should see a gradual decrease in the SFR resulting in an “ageing” behaviour (a gradual decrease in star formation over a more extended time interval), rather than a sharp “quenching” (Casado et al. 2015; Corcho-Caballero et al. 2021), i.e. a sudden stop in star formation. Note, this is especially true as all our galaxies have late-type morphology. Therefore, owing to the slow “ageing” of galaxies, AGN and SF in the sample “twin” pairing (AGN B or C with SF D or E) should have line strengths that are indistinguishable between them if they had similar formation time, especially for $D_n(4000)$ and $[\text{MgFe}]'$ within this hypothesis. We emphasize that differences could also be due to a substantial difference in the evolutionary stage, for instance, pairing AGN B or C with SF A or B, in Fig. 11.

this behaviour, with a schematic diagram of the variation in the Eddington ratio of the SMBH (f_{Edd}), in green, throughout a galaxy’s life cycle. The dots give examples of galaxies that will be identified as AGN (black) or SF (blue) when classified on the BPT diagram, respectively. In the “on-off” model, the behaviour in f_{Edd} will rapidly quench star formation when the AGN is in an “on” mode (high f_{Edd}), at least within the central region, resuming the star formation activity once it goes back to the “off” mode (low f_{Edd}) - depending on whether enough gas available for star formation is left over. This “on-off” behaviour operates over timescales that are much shorter than the sensitivity of line strengths, and even emission lines (from the ionising photons of massive stars). Therefore, we should see a gradual decrease in the SFR resulting in an “ageing” behaviour (a gradual decrease in star formation over a more extended time interval), rather than a sharp “quenching” (Casado et al. 2015; Corcho-Caballero et al. 2021), i.e. a sudden stop in star formation. Note, this is especially true as all our galaxies have late-type morphology. Therefore, owing to the slow “ageing” of galaxies, AGN and SF in the sample “twin” pairing (AGN B or C with SF D or E) should have line strengths that are indistinguishable between them if they had similar formation time, especially for $D_n(4000)$ and $[\text{MgFe}]'$ within this hypothesis. We emphasize that differences could also be due to a substantial difference in the evolutionary stage, for instance, pairing AGN B or C with SF A or B, in Fig. 11.

G1 features the largest variation between AGN and SF systems, where AGN galaxies, measured within a $1.5''$ aperture, reside near the RS (AGN D) but SF galax-

ies reside either in the BC or GV. In addition, G1 twins display a greater radial difference between the central region and the largest aperture, $1.5 R_{\text{eff}}$, for AGN galaxies, with respect to the SF counterparts (see Fig. 7 and Fig. 8). Fig. 9 also shows generally an older population in the central region for AGN galaxies with respect to their SF counterpart. Such behaviour seems antithetical to the “on-off” AGN mode, however it can still be applicable, provided the AGN twin has a different formation time compared to the SF equivalent. This could hint towards the AGN galaxy being formed earlier than their SF twin counterpart, as our selection criteria does not match for formation time. Therefore, these AGN galaxies may be in a state closer to the end of their AGN life cycle, whereas the SF galaxies – while still experiencing some form of AGN activity – have been formed in more recent cosmological times. The G4 twin further supports this idea, as the AGN is located close to the GV but their SF galaxy is located in the BC. However, since the AGN galaxy can be thought of as just entering the GV, we can assume it lies in a state more representative of the middle of its AGN life-cycle (AGN B or C), resulting in similar properties between AGN and SF counterparts – unlike the G1 twins (see Fig. 7 and 8). Finally, galaxies in both G1 and G4 have bars, which is thought to play an important role with conjunction to AGN to quenching of star formation (see, e.g., Ellison et al. 2011; Sánchez-Blázquez et al. 2011). However, the interpretation of such results is beyond the scope of this paper.

G2 and G3 twins have AGN and SF galaxies with more similar population properties, regardless of the aperture size. There is no clear distinction between AGN and SF galaxies at the central region or in the largest aperture (see Fig. 7 and 8), favouring the “on-off” AGN hypothesis, where both AGN and SF galaxies have similar formation time (as in AGN B or C paired with SF D or E in Fig. 11). G2 and G3 twins show similar behaviour between their AGN and SF galaxies, however this could be due to different reasons. G2 twins are both old, have very weak $H\alpha$ emission, and are classified as Sa, thus featuring prominent central bulges. These properties indicate that the AGN in G2 may be undergoing maintenance mode activity (Barišić et al. 2019), explaining the similarity found in the stellar populations of AGN and SF twin pairs. In contrast, G3 twins have strong $H\alpha$ emission lines for both AGN and SF members and they are classified as late spirals. Therefore rather than invoking maintenance mode, we can think of these galaxies as undergoing more active “on-off” events at the start or middle of the AGN life cycle. Additionally, the analysis of the SSP equivalent ages (Fig. 9) gives no clear difference between AGN and SF galaxies. Note that previous studies, such as Lacerda et al. (2020) and A19, noted AGN hosts are more evolved than SF galaxies, as the former are mainly located in the GV, whereas the latter mostly reside in the BC. However, in the comparison between this targeted set of twin galaxies, this behaviour seems less clear. Within the “on-off” AGN hypothesis, this contrast should be due to their different formation times.

4.4 “no-AGN” hypothesis

At low and intermediate stellar mass ($M_{\star} \lesssim 10^{10.3} M_{\odot}$) there is ample evidence suggesting that stellar feedback and environmental mechanisms are sufficient to quench star for-

mation (Feldmann et al. 2010; Naab et al. 2014). However, at the massive end, AGN activity has been necessary to explain quiescent galaxies (Silk & Rees 1998; Nelson et al. 2018). We propose an alternative simple model, which is an alternative to the “on-off” model, to explain the properties of the twin pairs. In the “no-AGN” hypothesis we assume that, within same stellar mass, some galaxies will quench their star formation through AGN activity while others will (i) not experience any AGN (ii) will not quench their SF through AGN but through different physical mechanisms such as stellar feedback or morphological quenching mechanisms. This scenario would imply that in twin galaxies, we should find statistically significant differences between the stellar populations of AGN and SF twin pairs. Previous work in the literature, such as del Moral-Castro et al. (2019) and del Moral-Castro et al. (2020), have found strong evidence supporting the “no-AGN” hypothesis, where they find AGN galaxies to consistently display higher angular momentum than their SF counterpart. Note that variations in angular momentum are related to larger timescales, that cannot be explained in the context of a simple “on-off” AGN switch model (assuming similar formation time for these “twin” systems), as the AGN duty cycle is rather short-lived, of order $\sim 10^5$ yr. Similarly, these short timescales are not sufficient enough to explain the line strength differences we observe, as stellar population indicators vary over timescales of order ~ 100 Myr.

In this work, the analysis of G1 twins generally shows older populations in AGN galaxies (Fig. 9). This trend, while possible, would be unlikely, if we were to assume a simple “on-off” scenario. The estimation of SSP metallicity, Fig. 10, shows AGN galaxies are generally more metal rich compared to their SF counterparts, within $1.5''$ and 2.2 kpc apertures. Once more, such variation in metallicity is expected over longer timescales ($\gg 100$ Myr), indicating a different chemical enrichment history, which implies timescales that are longer than those expected in the “on-off” AGN switching mode. The analysis of the G4 twin yields a similar result, where we find the metallicity of AGN galaxies consistently greater than their SF counterpart.

We emphasize the diversity found among galaxies in such a small sample, reflecting the subtle role of AGN quenching over the timescales that can be probed with stellar population studies. While we find evidence supporting both models presented here, a larger set of twin pairs is needed to assess the validity of the two alternative hypotheses.

5 SUMMARY

In this paper, we have investigated the stellar population properties of a carefully defined state-of-the-art sample of twin galaxies (del Moral-Castro et al. 2020), selected from the CALIFA IFU survey. Galaxies in twins are expected to appear undistinguishable from the point of view of size, mass, morphology and inclination, with the only difference being the presence or absence of an AGN. We project this sample onto a dust resilient evolutionary plane spanned by $D_n(4000)$ vs stellar mass; following the methodology outlined in A19. The original 11 twin sample (20 twin pairs) is reduced to 8 twins (10 twin pairs), due to a new se-

lection criteria restricting differences in velocity dispersion and stellar mass, to maximise the similarities between twins concerning the stellar populations. We study stacked spectra within three different apertures – the most central region, ($R \leq 1.5''$), a region that matches, on average, the single fibre of the SDSS legacy spectra at $0.05 \lesssim z \lesssim 0.1$ ($R \leq 2.2$ kpc), and a much more extended aperture, probing out to $R \leq 1.5 R_{\text{eff}}$. We find similar fractions of AGN (6/8 - *NGC1093*, *NGC2639*, *NGC2906*, *NGC2916*, *NGC6394* and *NGC7466*) and SF (5/7 - *NGC5947*, *NGC2253*, *NGC6004*, *NGC2916*, *NGC0160*) galaxies to reside in the GV, within 2.2 kpc aperture. However, we find evidence of the role of AGN in quenching, as AGN galaxies in a twin system have greater $D_n(4000)$ than their SF counterpart 90% of the time, regardless of aperture size (Fig. 2).

The sample is divided into a set of groups depending on their location in this diagram (i.e. whether they live on the RS, GV, or BC) finding diverse sets of grouping. We base this classification on spectra in the most central (1.5'') aperture as AGN activity is thought to impact more significantly the immediate vicinity. We grouped twins 1, 3 and 4 into group G1 as they all have their AGN in the RS, while the SF counterpart resides in the BC. Similarly, group G2 (twin 2 and 5) have their AGN in the RS but the SF system also resides in the RS. Group G3 (twin 7 and 8) have both AGN and SF in the GV. Finally, G4 (twin 5) has the AGN in the GV, while the SF galaxies are in the BC.

The twin sample is compared with a general distribution of galaxies from SDSS, with similar stellar mass. All twin AGN galaxies were selected in the CALIFA sample as type 2 Seyfert AGN, therefore, we need to select the same type in the SDSS sample. We separate type 1 and 2 AGN in the Seyfert sample from SDSS. This novel method makes use of the equivalent width of the $H\alpha$ line in SF galaxies, to calibrate the peak of $H\alpha$ emission in lines without a broad component.

Furthermore, statistical tests show all twin galaxies have a relative difference within 3σ and all but one twin had difference within 1σ for randomly selected galaxies of only SF type or SF and AGN type (Fig. 6). Note, due to the small sample size, we do not find any strong conclusive results. However, we always find the relative variation to be positive, $\gtrsim 0$, indicating, to a minor degree, a consistent physical difference caused by the AGN activity. Therefore, this study should be treated more as a *pilot study*, which motivates the extension of this methodology to a larger sample to confirm, and draw a strong conclusion on whether such positive difference between “twin” samples is due to the effect of the AGN on the evolution of the star formation history of galaxies.

The analysis of a targeted set of line strengths showed a mixture of behaviour regarding the stellar populations. These results were discussed in the framework of two alternative hypothesis, one invoking the “on-off” switching of the AGN, and the other assuming that while in some galaxies the AGN exerts the dominant form of quenching, in others quenching is not related to AGN activity - named “no-AGN”. AGN galaxies generally have stronger 4000\AA break and $[\text{MgFe}]'$ and weaker $H\delta_A$ within 1.5'' and 2.2 kpc aperture – indicating an older and more metal rich population. However, converting these line strengths to SSP equivalent ages and metallicities shows there is no clear trend in stellar

age between AGN and SF galaxies (Fig. 9). In contrast to age, 70%, 80% and 70% of AGN galaxies appear more metal rich within 1.5'', 2.2 kpc and 1.5 R_{eff} (Fig. 10), respectively indicating even amongst “twin” sample AGN galaxies have a different formation time or star formation and chemical enrichment histories. The assumption of different formation time would fit the “on-off” AGN hypothesis, while the different star formation and chemical evolution histories would support the “no-AGN” scenario.

Finally, the presence of a bar may play an important role, as we can rearrange the grouped twins into sets where groups 1 and 4 have a bar and groups 2 and 3 are galaxies without bar. Groups 1 and 4 feature consistent differences between AGN and SF galaxies, mostly supporting the no-AGN theory or suggesting a different formation time, whereas groups 2 and 3, show more similarities than differences between AGN and SF galaxies, supporting the “on-off” AGN switching mode hypothesis. The diversity of the results in this sample shows the complex behaviour, thus no definitive conclusion can be drawn. However, this work provides a strong justification for a larger study that adopts the methodology implemented in this paper - with upcoming surveys owing to the difficulty of finding “twin” galaxies - to study the effect of AGN on the evolution of star formation in galaxies.

6 ACKNOWLEDGEMENTS

The referee, Yago Ascasibar, is thanked for his constructive criticism. JA is supported by the UK Science and Technology Facilities Council (STFC). IMC acknowledges the support of the Instituto de Astrofísica de Canarias via an Astrophysicist Resident fellowship. We acknowledge support from the Spanish Ministry of Science, Innovation and Universities (MCIU), through grant PID2019-104788GB-I00 (IF). BG-L acknowledges support from the Spanish Ministry of Science, Innovation and Universities (MCIU), Agencia Estatal de Investigación (AEI), and the Fondo Europeo de Desarrollo Regional (EU-FEDER) under projects with references AYA20155-68217-P and PID2019-107010GB-I00. CRA acknowledges financial support from the Spanish Ministry of Science, Innovation and Universities (MCIU) under grant with reference RYC-2014-15779, from the European Union’s Horizon 2020 research and innovation programme under Marie Skłodowska-Curie grant agreement No 860744 (BiD4BEST), from the State Research Agency (AEI-MCINN) of the Spanish MCIU under grants “Feeding and feedback in active galaxies” with reference PID2019-106027GB-C42, “Feeding, feedback and obscuration in active galaxies” with reference AYA2016-76682-C3-2-P, and “Quantifying the impact of quasar feedback on galaxy evolution (QSOFEED)” with reference EUR2020-112266. CRA also acknowledges support from the Consejería de Economía, Conocimiento y Empleo del Gobierno de Canarias and the European Regional Development Fund (ERDF) under grant with reference ProID2020010105 and from IAC project P/301404, financed by the Ministry of Science and Innovation, through the State Budget and by the Canary Islands Department of Economy, Knowledge and Employment, through the Regional Budget of the Autonomous Community. This study uses data provided by

the Calar Alto Legacy Integral Field Area (CALIFA) survey (<http://califa.caha.es/>). Based on observations collected at the Centro Astronómico Hispano Alemán (CAHA) at Calar Alto, operated jointly by the Max-Planck-Institut für Astronomie and the Instituto de Astrofísica de Andalucía (CSIC). Funding for SDSS-III has been provided by the Alfred P. Sloan Foundation, the Participating Institutions, the National Science Foundation, and the U.S. Department of Energy Office of Science. The SDSS-III web site is <http://www.sdss3.org/>.

7 DATA AVAILABILITY

The data regarding SDSS (<http://skyserver.sdss.org/dr16>) and CALIFA (<https://califa.caha.es>) data, used in this paper is publicly available at the respective websites. The data used for this project is available upon reasonable request.

REFERENCES

- Abolfathi B., et al., 2018, *ApJs*, 235, 42
- Anghopo J., Ferreras I., Silk J., 2019, *MNRAS*, 488, L99
- Anghopo J., Ferreras I., Silk J., 2020, *MNRAS*
- Anghopo J., Negri A., Ferreras I., de la Rosa I. G., Dalla Vecchia C., Pillepich A., 2021, *MNRAS*, 502, 3685
- Antonucci R., 1993, *ARA&A*, 31, 473
- Baldry I. K., Glazebrook K., Brinkmann J., Ivezić Ž., Lupton R. H., Nichol R. C., Szalay A. S., 2004, *ApJ*, 600, 681
- Baldwin J. A., Phillips M. M., Terlevich R., 1981, *PASP*, 93, 5
- Balogh M. L., Morris S. L., Yee H. K. C., Carlberg R. G., Ellingson E., 1999, *ApJ*, 527, 54
- Barišić I., et al., 2019, *ApJ*, 872, L12
- Barnes J. E., Hernquist L. E., 1991, *ApJ*, 370, L65
- Barrera-Ballesteros J. K., et al., 2014, *A&A*, 568, A70
- Bell E. F., 2008, *ApJ*, 682, 355
- Bitsakis T., et al., 2019, *MNRAS*, 483, 370
- Breda I., et al., 2020, *A&A*, 635, A177
- Bremer M. N., et al., 2018, *MNRAS*, 476, 12
- Brinchmann J., Charlot S., White S. D. M., Tremonti C., Kauffmann G., Heckman T., Brinkmann J., 2004, *MNRAS*, 351, 1151
- Bruzual G., Charlot S., 2003, *MNRAS*, 344, 1000
- Bundy K., et al., 2015, *ApJ*, 798, 7
- Cappellari M., Emsellem E., 2004, *PASP*, 116, 138
- Cappellari M., et al., 2011, *MNRAS*, 413, 813
- Cardelli J. A., Clayton G. C., Mathis J. S., 1989, *ApJ*, 345, 245
- Casado J., Ascasibar Y., Gavilán M., Terlevich R., Terlevich E., Hoyos C., Díaz A. I., 2015, *MNRAS*, 451, 888
- Catalán-Torrecilla C., et al., 2015, *A&A*, 584, A87
- Cid Fernandes R., Mateus A., Sodré L., Stasińska G., Gomes J. M., 2005, *MNRAS*, 358, 363
- Cid Fernandes R., Stasińska G., Schlickmann M. S., Mateus A., Vale Asari N., Schoenell W., Sodré L., 2010, *MNRAS*, 403, 1036
- Cisternas M., et al., 2011, *ApJ*, 726, 57
- Conroy C., Gunn J. E., 2010, *ApJ*, 712, 833
- Corcho-Caballero P., Casado J., Ascasibar Y., García-Benito R., 2021, *MNRAS*, 507, 5477
- Correa C. A., Schaye J., Trayford J. W., 2019, *MNRAS*, 484, 4401
- Croom S. M., et al., 2021, *MNRAS*,
- Croton D. J., et al., 2006, *MNRAS*, 365, 11
- Dashyan G., Choi E., Somerville R. S., Naab T., Quirk A. C. N., Hirschmann M., Ostriker J. P., 2019, *MNRAS*, p. 1710
- del Moral-Castro I., et al., 2019, *MNRAS*, 485, 3794
- del Moral-Castro I., et al., 2020, *A&A*, 639, L9
- Díaz-García L. A., et al., 2019, *A&A*, 631, A156
- Ellison S. L., Nair P., Patton D. R., Scudder J. M., Mendel J. T., Simard L., 2011, *MNRAS*, 416, 2182
- Faber S. M., et al., 2007, *ApJ*, 665, 265
- Falcón-Barroso J., et al., 2006, *MNRAS*, 369, 529
- Feldmann R., Carollo C. M., Mayer L., Renzini A., Lake G., Quinn T., Stinson G. S., Yepes G., 2010, *ApJ*, 709, 218
- Ferreras I., Charlot S., Silk J., 1999, *ApJ*, 521, 81
- Ferreras I., et al., 2019, *MNRAS*, 489, 608
- Gkini A., Plionis M., Chira M., Koulouridis E., 2021, arXiv e-prints, p. [arXiv:2101.01481](https://arxiv.org/abs/2101.01481)
- Graves G. J., Faber S. M., Schiavon R. P., Yan R., 2007, *ApJ*, 671, 243
- Graves G. J., Faber S. M., Schiavon R. P., 2010, *ApJ*, 721, 278
- Gunn J. E., et al., 2006, *AJ*, 131, 2332
- Hayward C. C., Hopkins P. F., 2017, *MNRAS*, 465, 1682
- Heckman T. M., Best P. N., 2014, *ARA&A*, 52, 589
- Ho L. C., 2008, *ARA&A*, 46, 475
- Ji X., Yan R., Riffel R., Drory N., Zhang K., 2020, *MNRAS*, 496, 1262
- Kalinova V., Colombo D., Sánchez S. F., Kodaira K., García-Benito R., González Delgado R., Rosolowsky E., Lacerda E. A. D., 2021, arXiv e-prints, p. [arXiv:2101.10019](https://arxiv.org/abs/2101.10019)
- Kaviraj S., et al., 2007, *ApJS*, 173, 619
- Kelvin L. S., et al., 2018, *MNRAS*, 477, 4116
- Kewley L. J., Dopita M. A., Sutherland R. S., Heisler C. A., Trevena J., 2001, *ApJ*, 556, 121
- Kewley L. J., Dopita M. A., Leitherer C., Davé R., Yuan T., Allen M., Groves B., Sutherland R., 2013, *ApJ*, 774, 100
- Kewley L. J., Nicholls D. C., Sutherland R. S., 2019, *ARA&A*, 57, 511
- Kocevski D. D., et al., 2012, *ApJ*, 744, 148
- Kormendy J., Ho L. C., 2013, *ARA&A*, 51, 511
- La Barbera F., Ferreras I., Vazdekis A., de la Rosa I. G., de Carvalho R. R., Trevisan M., Falcón-Barroso J., Ricciardelli E., 2013, *MNRAS*, 433, 3017
- Lacerda E. A. D., Sánchez S. F., Cid Fernandes R., López-Cobá C., Espinosa-Ponce C., Galbany L., 2020, *MNRAS*, 492, 3073
- Lacerna I., Ibarra-Medel H., Avila-Reese V., Hernández-Toledo H. M., Vázquez-Mata J. A., Sánchez S. F., 2020, *A&A*, 644, A117
- Li C., et al., 2015, *ApJ*, 804, 125
- Lintott C. J., et al., 2008, *MNRAS*, 389, 1179
- Lipari S., Colina L., Macchetto F., 1994, *ApJ*, 427, 174
- Marinacci F., et al., 2018, *MNRAS*, 480, 5113
- Martin D. C., et al., 2007, *ApJ*, 173, 342
- Mathews W. G., Baker J. C., 1971, *ApJ*, 170, 241
- Méndez-Abreu J., et al., 2017, *A&A*, 598, A32
- Naab T., et al., 2014, *MNRAS*, 444, 3357
- Nelson D., et al., 2018, *MNRAS*, 475, 624
- Phillipps S., et al., 2019, *MNRAS*, 485, 5559
- Pillepich A., et al., 2018, *MNRAS*, 473, 4077
- Ramos Almeida C., et al., 2011, *ApJ*, 731, 92
- Salim S., 2014, *Serb. Astron. J.*, 189, 1
- Sánchez-Blázquez P., Ocvirk P., Gibson B. K., Pérez I., Peletier R. F., 2011, *MNRAS*, 415, 709
- Sánchez S. F., et al., 2012, *A&A*, 538, A8
- Sánchez S. F., et al., 2016, *A&A*, 594, A36
- Sánchez S. F., et al., 2018, *Rev. Mex. Astron. Astrofis.*, 54, 217
- Sarzi M., et al., 2006, *MNRAS*, 366, 1151
- Schawinski K., Thomas D., Sarzi M., Maraston C., Kaviraj S., Joo S.-J., Yi S. K., Silk J., 2007, *MNRAS*, 382, 1415
- Schawinski K., et al., 2014, *MNRAS*, 440
- Schawinski K., Koss M., Berney S., Sartori L. F., 2015, *MNRAS*, 451, 2517
- Schaye J., et al., 2015, *MNRAS*, 446, 521
- Schimionovich D., et al., 2007, *ApJ*, 173, 315

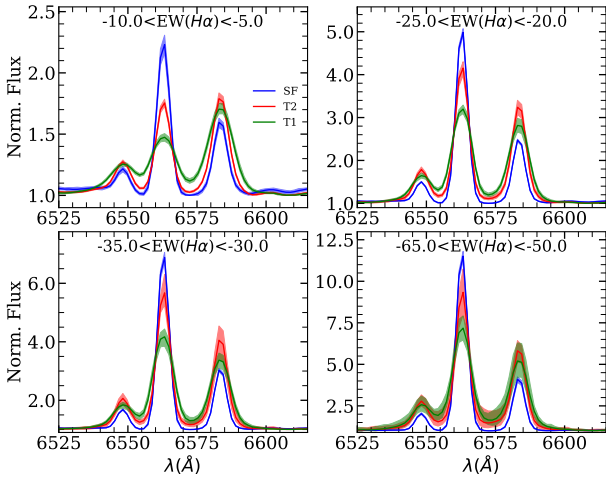


Figure A1. Stacked spectra of galaxies in the $H\alpha+[NII]$ region, classified as either star-forming (blue, SF), type 1 (green, T1) and type 2 (red, T2) AGN. The stacks corresponding to AGN (SF) galaxies consist of 30% (5%) of the total galaxies in the $EW(H\alpha)$ bins.

- Silk J., Rees M. J., 1998, *A&A*, **331**, L1
 Simmons B. D., et al., 2013, *MNRAS*, **429**, 2199
 Smee S. A., et al., 2013, *AJ*, **146**, 32
 Soltan A., 1982, *MNRAS*, **200**, 115
 Spindler A., et al., 2018, *MNRAS*, **476**, 580
 Spinoglio L., Fernández-Ontiveros J., 2021, *IAU Symposium*, **356**, 29
 Springel V., et al., 2017, *MNRAS*, **475**, 676
 Springel V., et al., 2018, *MNRAS*, **475**, 676
 Strateva I., et al., 2001, *AJ*, **122**, 1861
 Tachella S., et al., 2015, *Science*, **348**, 314
 Terrazas B. A., et al., 2020, *MNRAS*, **493**, 1888
 Thomas D., Maraston C., Schawinski K., Sarzi M., Silk J., 2010, *MNRAS*, **404**, 1775
 Vazdekis A., Ricciardelli E., Cenarro A. J., Rivero-González J. G., Díaz-García L. A., Falcón-Barroso J., 2012, *MNRAS*, **424**, 157
 Vazdekis A., Koleva M., Ricciardelli E., Röck B., Falcón-Barroso J., 2016, *MNRAS*, **463**, 3409
 Villarroel B., Korn A. J., 2014, *Nature Physics*, **10**, 417
 Walcher C. J., et al., 2014, *A&A*, **569**, A1
 White S. D. M., Frenk C. S., 1991, *ApJ*, **379**, 52
 Williams R. J., Quadri R. F., Franx M., van Dokkum P., Labbé I., 2009, *ApJ*, **691**, 1879
 Worthey G., 1994, *ApJS*, **95**, 107
 Wright R. J., Lagos C. d. P., Davies L. J. M., Power C., Trayford J. W., Wong O. I., 2019, *MNRAS*, **487**, 3740
 Wyder T. K., et al., 2007, *ApJS*, **173**, 293
 York D. G., et al., 2000, *AJ*, **120**, 1579

APPENDIX A: TYPE 1 AND 2 AGN AND SF GALAXY SPECTRA

We test here the validity of the approach followed in Sec. 2.4 to further classify SDSS spectra flagged as Seyfert AGN (BPT flag 4 in the GALSPECXTRA catalogue) into type 1 and type 2. The criterion is based on a comparison between line amplitude and equivalent width (Fig. 1), so that the AGN sample that closely follows the trend of star-forming

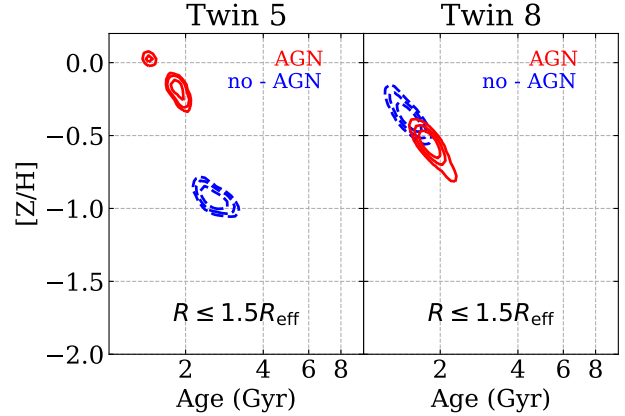


Figure B1. Confidence levels of the SSP-equivalent age and metallicity corresponding to galaxies in twin 8, using the largest ($R \leq 1.5R_{\text{eff}}$) aperture. The contours represent, from the inside out the 1, 2 and 3 σ levels. Solid red and dashed blue contours show the results for the AGN and SF galaxy, respectively.

galaxies (BPT flag 1) is supposed to be type 2 AGN, i.e. lacking a broad component. Fig. A1 shows the stacked spectra of SF, type 1 and 2 AGN for different bins of $EW(H\alpha)$ in blue, green and red, respectively (following the same colour scheme as Fig. 1). For each bin, we make 50 stacks, consisting of 30% of type 1 and 2 AGN galaxies and 5% of SF galaxies. We then plot the mean spectrum, where the errorbar (filled colour) indicates the minimum and maximum flux in each stack at a given wavelength. The spectra are normalised in the displayed spectral window, dividing it by the minimum flux in each individual stack. The figure illustrates the expected trend, where galaxies classified as type 1 have a clear signature of a broad component. At the lowest $EW(H\alpha)$, where we have the highest number of galaxies, we find the cleanest separation, where the green line features a wider $H\alpha$ line compared to both red and blue lines. This is also evident at higher $EW(H\alpha)$, but there are fewer galaxies with a broad component (type 1) in this case.

APPENDIX B: AGE-METALLICITY DEGENERACY

The line strengths are all prone to the age-metallicity degeneracy (Worthey 1994), therefore affecting the estimation of our SSP equivalent ages and metallicities. This degeneracy implies that the effect of an old stellar population can be mimicked by a higher metallicity, producing very similar colours or even line strengths (Ferrerias et al. 1999). To break such degeneracy, we make use of a battery of line strengths with different sensitivity to age and chemical composition. Our set of indices comprises: $D_n(4000)$, $H\delta_A$, $H\gamma_A$, Mgb , $Fe5270$, $Fe5335$ and $[MgFe]$. The spectra have a high S/N, which helps to break such degeneracy. Fig. B1 shows a bivariate plot with the confidence levels for the SSP-equivalent age and metallicity of twin 5 and 8. The contours are shown – from the inside out – at the 1, 2, and 3 σ level. The solid red (dashed blue) contours correspond to the twin with (without) an AGN. A large overlap between these contours would mean a substantial age-metallicity degeneracy, so that the

best-fit SSP parameters would be affected by it. We find no overlap between AGN and SF contours for twin 5, indicating that similar trends to twin 5 in $R \leq 1.5 R_{\text{eff}}$ should be independent of the age-metallicity degeneracy. Twin 8 shows some level of overlap between the contours, indicating there might be some level of degeneracy, however within 1σ we find there to be no overlap in confidence levels, therefore indicating that the difference in age/metallicity is robust. Furthermore, our χ^2 analysis consists of artificially boosting the uncertainty by adding, in quadrature, 5% of the index value due to our models not being accurate enough to explain the observations. Therefore, our confidence level should be tighter, thus breaking the age-metallicity degeneracy, as we are unlikely to have large overlaps on the contours.

APPENDIX C: CHOICE OF APERTURES

In order to assess the effect of AGN activity on its host galaxy, we study the stellar population properties of galaxies at various apertures. Fig. C1 shows the 3 apertures we have chosen to analyse the stellar populations, quoted in terms of radius $R \leq 1.5''$, $R \leq 2.2 \text{ kpc}$ and $R \leq 1.5 R_{\text{eff}}$. The spectra from individual spaxels, with $S/N \geq 3$, are summed up within each aperture, leading to high signal to noise ratio, $S/N \geq 100$. Additionally, the spectra are brought to rest-frame using the velocity maps computed in del Moral-Castro et al. (2020).

APPENDIX D: GALAXY SDSS IMAGES

Here we display stamp-like images, obtained from the CALIFA collaboration using SDSS images, of the various twins (Fig. D1 and Fig. D2). Each row corresponds to a twin pairing, where the left-most galaxy is an AGN, while the rest are SF. For the different groups identified in this paper, we have framed the respective twins accordingly. G1, G2, G3 and G4 twins are framed in black, red, blue and green, respectively.

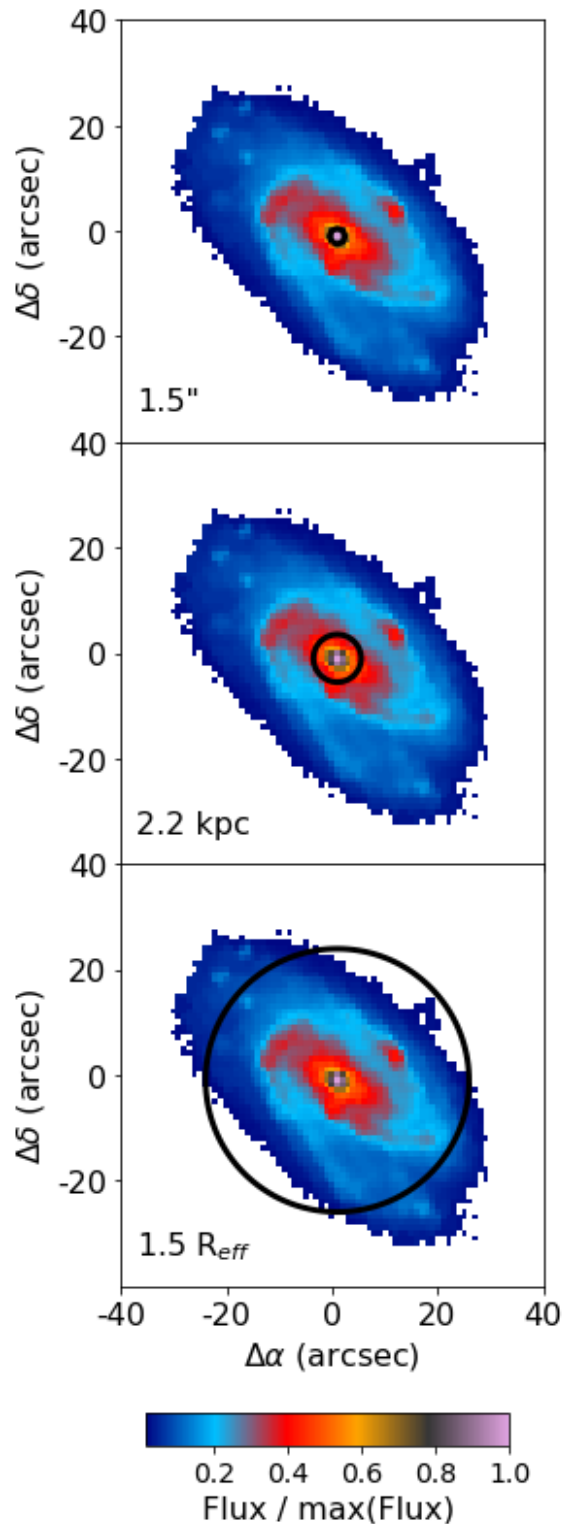


Figure C1. Stellar flux map, UGC00005, of a data cube from the CALIFA survey. *Top, middle and bottom:* panels show in black the most central radial aperture, $R \leq 1.5''$, radial aperture to match the SDSS survey, $R \leq 2.2 \text{ kpc}$, and maximum radial aperture, $R \leq 1.5 R_{\text{eff}}$, respectively.

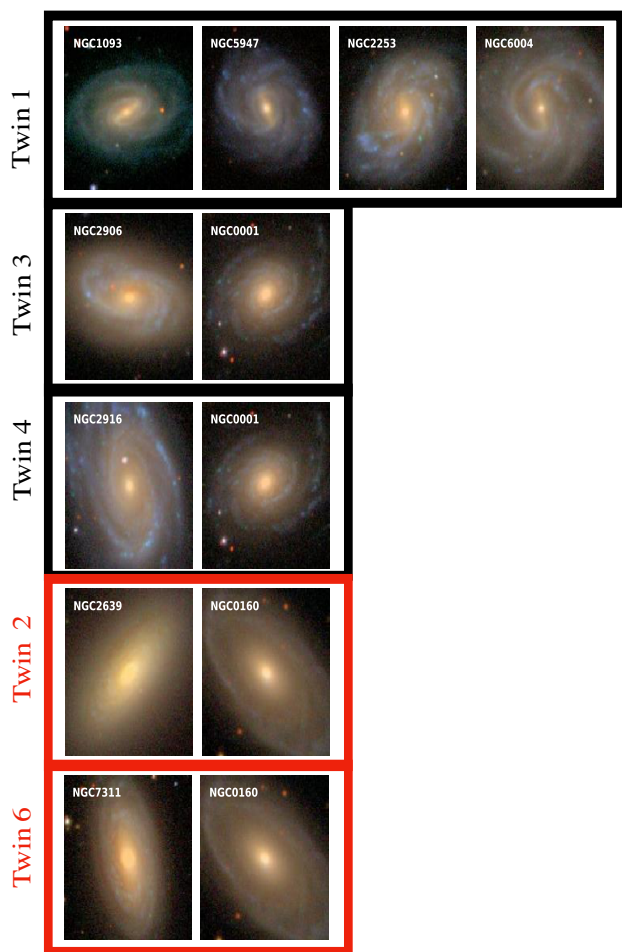


Figure D1. Colour-composite SDSS images of the active galaxies (left column) and their corresponding non-active twin(s). Each image has a field of view of $90'' \times 90''$. North is up and east to the left. The frame colour indicates the group that each of the twin pair belongs to. Here, twins with black and red frames indicate G1 and G2 galaxies, respectively.

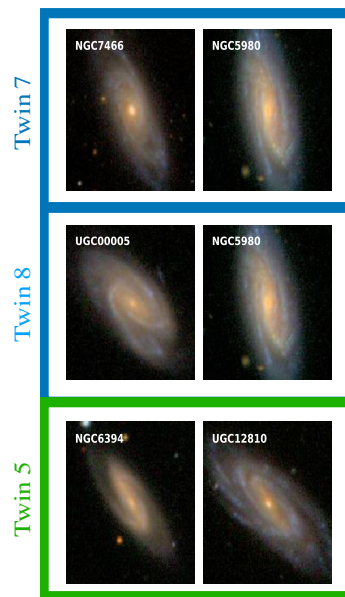


Figure D2. Continuation of Fig. D1. The blue and green frames indicate groups G3 and G4, respectively.